Active synthesis of collagen (I) homotrimer and matrisomal proteins in Dupuytren's fibrosis

Kate Williamson[a], Gabriella Cooper[a], Katie J. Lee[a], Emma L. Beamish[a], Deborah Simpson[b], Alan Carter[a], Jade A. Gumbs[a,c], Graham Cheung[d], Daniel Brown[a, d], Rob Pettitt[e], Eithne J. Comerford[a,c,e], Peter D. Clegg[a,c], Elizabeth G. Canty-Laird[a,c,*]

* Corresponding author (elizabeth.laird@liverpool.ac.uk)

[a] Department of Musculoskeletal and Ageing Science, Institute of Life Course and Medical Sciences, University of Liverpool, William Henry Duncan Building, 6 West Derby Street, Liverpool, L7 8TX, United Kingdom

[b] Technology Directorate, Centre for Proteome Research, Department of Biochemistry & Systems Biology, Institute of Systems, Molecular & Integrative Biology, University of Liverpool, Crown Street, Liverpool L69 7ZB

[c] The Medical Research Council Versus Arthritis Centre for Integrated Research into Musculoskeletal Ageing (CIMA)

[d] Liverpool University Hospitals NHS Foundation Trust, Liverpool, United Kingdom

[e] Institute of Infection, Veterinary and Ecological Sciences, Leahurst Campus, University of Liverpool, Chester High Road, Neston, CH64 7TE, United Kingdom

Abstract

Dupuytren's disease is a common fibroproliferative disease of the palmar fascia of the hand with severe cases treated surgically. The rate of disease recurrence following treatment is high and a continual production of matrisomal proteins could lead to disease recurrence. There is no animal model for Dupuytren's disease, but analysis of the surgically excised tissue provides an accessible means to study the mechanisms of human tissue fibrosis. Here we sought to determine how new synthesis and the composition of matrisomal proteins in Dupuytren's differs from normal palmar fascia samples, using metabolic labelling approaches and proteomics. Model non-fibrotic, but fibrous connective tissues, equine flexor tendon and canine cranial cruciate ligament, were used to analyse active collagen-1 protein synthesis in development, ageing and degenerative disease, where it was restricted to early development and ruptured tissue. Dupuytren's tissue was shown to actively synthesise type I collagen, a proportion of which comprised abnormal collagen (I) homotrimer (mean 14.3% ± 14.4), as well as fibronectin, matrix metalloproteinases (MMP2, MMP3) and their inhibitors; Tissue Inhibitor of Metalloproteinases 2 (TIMP2). Insulin-Like Growth Factor Binding Protein 7 (IGFBP7) was actively synthesised by Dupuytren's as well as control tissue. Label-free analysis implicated the TGFβ pathway in the matrisomal profile of Dupuytren's tissue whilst myocilin, a Wnt-pathway regulator, was noticeably more abundant in control samples. No collagen (I) neopeptides representing the major collagenase cleavage site were identified, however periostin neopeptides were abundant in Dupuytren's tissue and gelatin neopeptides in both tissue types. Synthesis of MMP-resistant collagen-1 homotrimer, together with altered TGFβ and Wnt signalling environments, could contribute to the persistence of the fibrotic tissue and disease recurrence following treatment.

Introduction

Fibrillar collagens, particularly type I, are the major structural component of fibrous connective tissue including palmar fascia (aponeurosis), tendon, ligament, and fibrotic tissue. In fibrous tissue string-like fibrils comprise arrays of collagen molecules. Excessive accumulation of fibrillar collagens impedes normal tissue function resulting in particularly poor outcomes in cardiac, pulmonary, kidney and liver fibrosis (Wynn, 2008; Zeisberg and Kalluri, 2013). Dupuytren's disease is a common fibroproliferative disorder of the palmar fascia of the hand, which has sex, age, geographic and racial differences; being most prevalent in, but not restricted to, older men of Northern European descent (Hindocha et al., 2009). The aetiology of Dupuytren's is similarly complex involving genetics; an autosomal dominance pattern with varying penetrance, links to other diseases such as diabetes, epilepsy and liver disease, and environmental factors including alcohol intake and smoking (Grazina et al., 2019).

The formation of fibrous tissue under the skin can cause of Dupuytren's patients can cause localised pain and discomfort whilst disease progression may prevent the digits from straightening, producing fixed flexion contractures. The disease severity is commonly measured by the degree of joint contraction (which can be monitored Tubiana staging), the number of digits involved and the presence of disease outside the hand; Ledderhose disease in the foot or Peyronie's disease in the penis (Dibenedetti et al., 2011; Hindocha et al., 2008).

Treatment options include surgery; fasciectomy (excising the diseased tissue) and dermofasciectomy (excising the disease tissue and overlying skin), percutaneous needle aponeurotomy (dividing the diseased tissue) and did include collagenase treatment (prior to withdrawal from several jurisdictions) (Soreide et al., 2018); with each treatment carrying varying success, complications and recurrence rates (Krefter et al., 2017). In patients with advanced disease and debilitating contractures, the gold standard treatment is open limited fasciectomy followed by physiotherapy to encourage range of movement (Worrell, 2012). Surgical complication rates increase with disease severity and range between 3-50% (Craxford and Russell, 2016), whilst recurrence in the same finger/thumb or disease progression in other digits is common (8-54%) (Worrell, 2012).

The fibrotic tissue in Dupuytren's can comprise a highly cellular 'nodule' region, which is thought to represent an active stage in the tissue pathogenesis and a 'cord' region, consisting of mature fibrillar collagen (Layton and Nanchahal, 2019). Disease pathogenesis has been divided into proliferative, involutional (contracting) and residual stages, with progressively decreasing cellularity and increasing alignment along directional lines of tension (Luck, 1959). Type III collagen is present at very low levels in normal palmar fascia, but is abundant in Dupuytren's tissue (Brickley-Parsons et al., 1981). However, the proportion of type III collagen relative to total collagen decreases through the stages of disease progression from >35% to <20% in the residual stage (Lam et al., 2010). Myofibroblasts are abundant in nodules, display persistent alpha-smooth muscle actin (alpha-SMA) expression and are responsible for both matrix deposition and contraction. Bidirectional actin-fibronectin interactions (Tomasek and Haaksma, 1991) result in the progressive tensioning of collagen fibres and a concurrent increase in total flexion deformity (Verjee et al., 2009). Other cell types implicated in the initiation or progression of Dupuytren's fibrosis include embryonic stem cells, mesenchymal stromal cells, fibrocytes and immune cell populations (Layton and Nanchahal, 2019; Tan et al., 2018).

A systematic review of Dupuytren's disease 'omics' studies highlighted alterations in collagen and extracellular matrix (ECM) gene expression as well as genomic and transcriptomic studies implicating the TGFβ and Wnt signalling pathways in disease pathogenesis (Shih et al., 2012). One study has utilised proteomics in Dupuytren's disease and a two-dimensional gel electrophoresis approach implicated activation of the Akt signalling pathway as well as alterations in cytoskeletal proteins and those involved in

extracellular and intracellular signalling, oxidative stress and cellular metabolism (Kraljevic Pavelic et al., 2009).

Analysis of messenger RNA (mRNA) expression profiles in isolated Duputyren's fibroblasts found increased collagen and ECM mRNAs (Forrester et al., 2013), whilst a loss of collagen-regulating microRNAs (miRs) was identified in Dupuytren's tissue (Riester et al., 2015). A weighted gene co-expression network analysis and functional enrichment analysis of Dupuytren's transcriptomic datasets found gene ontology terms for ECM and collagen in ECM organisation, ECM-receptor interaction and collagen catabolic process, as well as adhesion and endoplasmic reticulum (ER) stress terms (Jung et al., 2019). An altered expression of matrix metalloproteinases (MMPs) has also been identified in Dupuytren's disease, as well as of a disintegrin and metalloproteinase domain with thrombospondin motif proteins (ADAMTSs) and tissue inhibitors of metalloproteinases (TIMPs), (Forrester et al., 2013; Johnston et al., 2007) whilst MMP14 variants are genetically linked to Dupuytren's (Ng et al., 2017).

Type I collagen molecules are predominantly $(\alpha1)_2(\alpha2)_1$ heterotrimers derived from the polypeptide gene products of the *COL1A1* and *COL1A2* genes. However, abnormal collagen $(\alpha1)_3$, homotrimer has been identified in Dupuytren's tissue (Ehrlich et al., 1982). Collagen (I) homotrimers are resistant to MMP-mediated proteolytic degradation (Makareeva et al., 2010) and may therefore skew the balance between collagen (I) synthesis and degradation, impeding the resolution of fibrosis.

We hypothesised that there may be a continual production of abnormal homotrimeric type I collagen or an altered profile of ECM that could contribute to the recurrence of Dupuytren's contracture following medical treatment. In this study, we utilised metabolic labelling approaches in combination with 1D gel electrophoresis or proteomics to analyse type I collagen and global protein synthesis and degradation in fibrotic Dupuytren's tissue, and in non-fibrotic but fibrous connective tissue. The study aimed to determine how new and residual fibrotic ECM differs from that produced in normal fibrous tissue and how collagen-1 synthesis differs from that seen in development, or tissue injury, with a view to identifying specific ECM proteins or pathways as targets for future anti-fibrotic therapy.

Methods

Sample collection

After full informed written consent (REC13/NW/0352 and REC 14/NW/0162), excised Dupuytren's tissue (fibrotic palmar fascia) and control non-diseased normal palmar fascia (PF), were taken from human patients undergoing surgery, at the Royal Liverpool and Broadgreen University Hospitals NHS Trust (now Liverpool University Hospitals NHS Foundation Trust) or the Warrington and Halton Hospitals NHS Foundation Trust (now Warrington and Halton Teaching Hospitals NHS Foundation Trust), for Dupuytren's contracture and Carpal tunnel syndrome respectively. Self-reported demographics were collected by questionnaire, and for the Dupuytren's patients disease stage information was collected from clinical records. Equine superficial digital flexor tendon (SDFT) and healthy canine cranial cruciate ligament (CCL) were collected as described (Ali et al., 2018; Lee et al., 2018), with local ethical approval (VREC186, VREC62 and RETH00000553). Ruptured CCL, otherwise discarded as clinical waste, was obtained from dogs undergoing stifle/knee stabilisation at the University of Liverpool's Small Animal Teaching Hospital (VREC63). Surgical samples were reserved in cold sterile saline and processed on the day of collection according to the selected analysis method.

Quantitative real-time PCR (qPCR)

Tissue samples were immersed in RNAlater (Qiagen) and stored at -20°C until analysis. The tissue was homogenised with a mikrodismembrator or a pestle and mortar in 1 ml of TRI Reagent® (Sigma-Aldrich, Poole, UK). 0.1 ml 1-bromo-3-chloropropane (BCP) (Sigma-Aldrich) was added to the homogenate and centrifuged for 15 minutes at 12,000 x g at 4°C. 1 µg of total RNA was reverse transcribed with M-MLV reverse transcriptase using random primers according to the manufacturer's protocol (Promega). RT-qPCR was performed in a 25 µl reaction volume containing; complementary DNA (cDNA) (5 ng), primers designed for the gene of interest (Table 1) and GoTaq(R) qPCR Master Mix (Promega). Samples were run on an AB 7300 Real Time PCR System (Applied Biosystems) using the following amplification conditions; 2 minutes at 95°C followed by 40 cycles of 15 seconds at 95°C and 1 minute at 60°C. Gene expression was calculated relative to GAPDH, which was determined to be a suitable reference gene after assessing its stability using the geNorm method.

Table 1: Primer Sequences

Species	Gene	Forward	Reverse
Human	COL1A1	GTTCAGCTTTGTGGACCTCCG	GATTGGTGGGATGTCTTCGTCT
	COL1A2	AGCCGGAGATAGAGGACCAC	AGCAAAGTTCCCACCGAGAC
	GAPDH	ATGGGGAAGGTGAAGGTCG	TAAAAGCAGCCCTGGTGACC
Equine	COL1A1	CATGTTCAGCTTTGTGGACCT	TGACTGCTGGGATGTCTTCTT
	COL1A2	CATGTTCAGCTTTGTGGACCT	TTTCCTGCAGTTGCCTCTTGT
	GAPDH	GCATCGTGGAGGGACTCA	GCCACATCTTCCCAGAGG
Canine	COL1A1	CCAGCCGCAAAGAGTCTACAT	TGACTGGTGGGATGTCTTCT
	COL1A2	ACAAGGAGTCTGCATGTCTAAGT	GCAGTTGCCTCCTGTAAAGA
	GAPDH	CTGGGGCTCACTTGAAAGG	CAAACATGGGGGCATCAG

Pulse-chase with ^{14}C-L-proline

Tissue samples were aseptically dissected into pieces, with an estimated wet weight of 25-50 mg or volume of ~25-50 µL each, under PBS or Dulbecco's minimal essential medium (DMEM), containing penicillin/streptomycin (1% v/v). After a 30-60 minute pre-equilibration at 37°C in DMEM containing penicillin/streptomycin (1% v/v), L-glutamine (2 mM), L-ascorbic acid 2-phosphate (200 µM) and β-aminopropionitrile (400 µM) (labelling media) with ~1-5 pieces per 1 ml of media, pulse–chase experiments were performed in labelling media supplemented with 2.5 µCi/ml [^{14}C]proline (GE Healthcare). After incubation in supplemented labelling media for 18 hrs, tissue samples were transferred to labelling media without [^{14}C]proline for 3 hrs. Subsequently, 1-2 tissue pieces were extracted in 100 µl aliquots of salt extraction buffer (1 M NaCl, 25 mM EDTA, 50 mM Tris-HCl, pH 7.4) containing protease inhibitors. Extracts were analysed by electrophoresis on 6% Tris-Glycine gels (ThermoFisher) with delayed reduction (Sykes et al., 1976) or on 4% Tris-Glycine gels (Invitrogen, discontinued) under reducing conditions. The gels were fixed in 10% methanol, 10% acetic acid, dried under vacuum, and exposed to a phosphorimaging plate (BAS-IP MS). Phosphorimaging plates were processed using a phosphorimager (Typhoon FLA7000 IP) and densitometry carried out using ImageQuant (GE Healthcare Life Sciences). The α1(I):α2(I) chain ratio was converted to a percentage homotrimeric collagen using the formula; (ratio-2)x100/ratio.

Metabolic labelling with $^{13}C_6$-L-lysine and mass spectrometry

Dupuytren's and normal palmar fascia dissections were performed aseptically under DMEM containing penicillin/streptomycin (1% v/v). Dupuytren's samples were dissected into cord and nodule regions after removal of any surrounding fatty tissue, and then cut into pieces with an estimated wet weight of 25-50 mg or volume of ~25-50 µL each. Normal PF samples were cut into two approximately equal sized pieces of a similar size. For each sample type, 1-2 tissue pieces were equilibrated in 1ml complete unlabelled SILAC media for 30 minutes at 37°C 5% CO_2 and then in 1ml complete [$^{13}C_6$]L-lysine labelled SILAC media (Lee et al., 2019) for 18-24 hours. Explants were then weighed, snap frozen and stored at -80°C whilst incubation medium was stored in aliquots at -20°C.

Tissue samples were disrupted using a Mikro-Dismembrator (Braun International) under liquid nitrogen. Approximately 10 mg of tissue was weighed directly into LoBind tubes (Eppendorf), snap frozen and stored at -80°C. For prior chondrotinase treatment, 80 µl of Chondroitinase ABC (AMSBIO AMS.E1028-10) at 1 U/ml in 100mM Tris Acetate containing protease inhibitors with EDTA was used per 10 mg of homogenized tissue and the chondroitinase supernatant reserved. A sequential GnHCl followed by 0.1% RapiGest extraction was carried out as described by (Ashraf Kharaz et al., 2017), except that 100 µl of GnHCl extraction buffer containing 1 mM EDTA was used per 10mg of starting material, the subsequent steps scaled similarly and the final Rapigest pellet extraction not carried out. For tissue extracts and chondroitinase supernatants filter-aided sample preparation (FASP) was carried out with centrifugation steps at 12,500 rpm for 15 minutes unless otherwise indicated. 100 µl of formic acid (1% v/v) was added to each filter (Vivacon 500, 10,000 MWCO, Sartorius) and spun. Extract from an equivalent of 2 mg of tissue or the entire chondroitinase supernatant was added to each filter and made up to 200 µl with 4M GnHCl in 50mM ammonium bicarbonate (GnHCl buffer). A 15-minute incubation in 8mM DTT in GnHCl buffer at 56°C in the dark with gentle vortexing preceded a 10-minute spin. Each filter was washed twice with 100 µl 4M GnHCl buffer and spun. 100 µl of 50mM iodoacetamide in GnHCl buffer was used to alkylate proteins with gentle vortexing and a 20-minute incubation in the dark before a 10-minute spin. Each filter was washed twice with 100ul GnHCl buffer, then thrice with 50mM ammonium bicarbonate with a 10-minute spin. Bound proteins were digested with 40 µl of trypsin at 10ng/µl in 47.5mM ammonium bicarbonate with 2.5mM acetic acid at 37°C overnight with steps to prevent evaporation, followed by a 10-minute spin and a subsequent wash with 40 µl of 50mM ammonium bicarbonate. Combined flow-throughs were acidified with Trifluoroacetic acid to 0.2% (v/v). Incubation media was bound to and digested off Strataclean beads as previously described (Angi et al., 2016; Ashraf Kharaz et al., 2017). A yeast enolase peptide standard was added to each sample, though this was not utilised for later quantification. Liquid chromatography tandem mass spectrometry (LC-MS/MS) was carried out as described (Lee et al., 2019) with loading volumes determined from prior ranging runs.

Proteomic data analysis

Protein identification, label-free quantification and analysis of $^{13}C_6$-L-lysine labelling was carried out as described (Lee et al., 2019) with the following modifications. *De novo* and database PEAKS searches were carried out using the UniHuman database with Waters Pepmix. Fragment mass error tolerance was set to 0.02 Da in searches and Proteins -10lgP ≥ 20 in filters. Results were normalized to the equivalent wet weight of tissue loaded on the trapping column or using the total ion chromatogram (TIC) and analysed using PeaksQ (Peaks Studio v8, Bioinformatics Solutions, Waterloo, Canada). The Dupuytren's:Normal PF ratio for each protein was calculated from group profile ratios as (Nodule+Cord)/(Normal PF x 2), converted to an expression fold change in IPA (Ingenuity Pathway Analysis, Qiagen) and used therein for analysis of upstream regulators. The Dupuytren's:Normal PF ratio was used to define proteins associated with each

tissue type for which protein interactions and pathways were analysed using STRING (Szklarczyk et al., 2019) using default settings.

Neopeptide analysis was carried out as described by (Peffers et al., 2014) with the following modifications. The UniHuman database was used and search parameters were enzyme; semiTrypsin, fragment mass tolerance; 0.01 Da, peptide charge; 2+, monoisotopic, instrument; ESI-QUAD-TOF and decoy selected. Peptide modifications were fixed carbamidomethyl cysteine, variable oxidation of methionine and variable heavy ($^{13}C_6$) lysine. Results were filtered for those neopeptides present in at least three normal PF samples or at least three cord and nodule samples

Statistical analysis

Data analysis was performed using SigmaPlot Version 14.0 and graphing carried out with GraphPad Prism 8 for Windows (GraphPad Software, La Jolla California USA, www.graphpad.com), unless otherwise indicated. Plots show individual data points together with the mean and +/- 1 SD unless otherwise indicated. COL1A1 and COL1A2 gene expression data was analysed using a Mann-Whitney rank sum test, whilst COL1A1:COL1A2 ratios were analysed using a t-test. For Bayesian analysis of the donor ages of samples analysed by qRT-PCR and proteomics, a free online Bayes factor calculator was used (http://www.lifesci.sussex.ac.uk/home/Zoltan_Dienes/inference/bayes_factor.swf) with a uniform age prior and upper and lower bounds of 75 and -75 respectively, to obtain a Bayes factor as described (Dienes, 2014). Polypeptide chain ratios were analysed using a one-sample t-test.

Principal components analysis (PCA) and associated graphing was carried out using Minitab® Statistical Software Version 18 (State College, PA: Minitab, Inc. (www.minitab.com)) as was Box-Cox data transformation. For PCA incorporating demographic data, self-reported textual data was coded in a binary manner except for diabetes - where diet-controlled (coded 1) was distinguished from type I (coded 2), smoking - where previous smokers were coded 1 and current smokers coded 2, alcohol consumption - where those consuming below the recommended limit were coded 1 and those above coded 2, and exercise - which was coded from 0-3 based on apparent intensity/duration.

For heavy lysine labelled peptides in media, a two-way ANOVA with tissue type and peptide as factors was used with a Holm-Sidak post-hoc test. Data failing the Shapiro-Wilk normality test and/or the Brown-Forsythe equal variance test was transformed using a Box-Cox transformation prior to analysis. Where a suitable transformation could not be found data were analysed using a Kruskal-Wallis one-way ANOVA on ranks with Dunn's pairwise comparisons.

Results

Collagen (I) homotrimer is actively produced by Dupuytren's tissue

To determine if collagen (I) homotrimer is continuously synthesized in Dupuytren's tissue, COL1A1 and COL1A2 gene expression was measured by qRT-PCR, and synthesis of α-chains by radiolabelling, in Dupuytren's samples and in normal PF controls. Expression of COL1A1 (Fig. 1A) and COL1A2 (Fig. 1B) was significantly higher in Dupuytren's tissue, indicative of new collagen (I) synthesis. The relative expression of COL1A1 as compared to COL1A2 was also higher in Dupuytren's tissue (Fig. 1C) indicating increased gene transcription and/or mRNA stability of COL1A1 as compared to COL1A2. There was no significant difference in the age of the Dupuytren's and normal PF samples that were analysed by qRT-PCR ($p=0.11$). A Bayesian analysis was used to determine if there was truly no difference in age between the groups, but results were inconclusive ($B=0.34$, insensitive).

Metabolic labelling with ^{14}C proline indicated Dupuytren's tissue explants but not normal PF controls (n=22) produced newly-synthesised collagen (I) protein (Fig. 1D). Samples derived from 27 of 31 Dupuytren's patients were sufficiently labelled for densitometric quantification (Supplementary Results). The α1(I):α2(I) chain ratio was significantly greater than 2 (Fig. 1E) indicative of new collagen (I) homotrimer synthesis. Using the ratios for the nodule only in the analyses (discounting 3 other cord samples) produced similar results (not shown). The α1(I):α2(I) ratio was converted to a percentage of homotrimeric collagen (I), indicating a mean value of 14.3% (SD ± 14.4%) and with one sample reading 50.4% (Fig. 1F). Plotting the α1(I):α2(I) ratio against the COL1A1:COL1A2 mRNA ratio indicated no direct correlation between relative mRNA and polypeptide chain ratios (Fig. 1G).

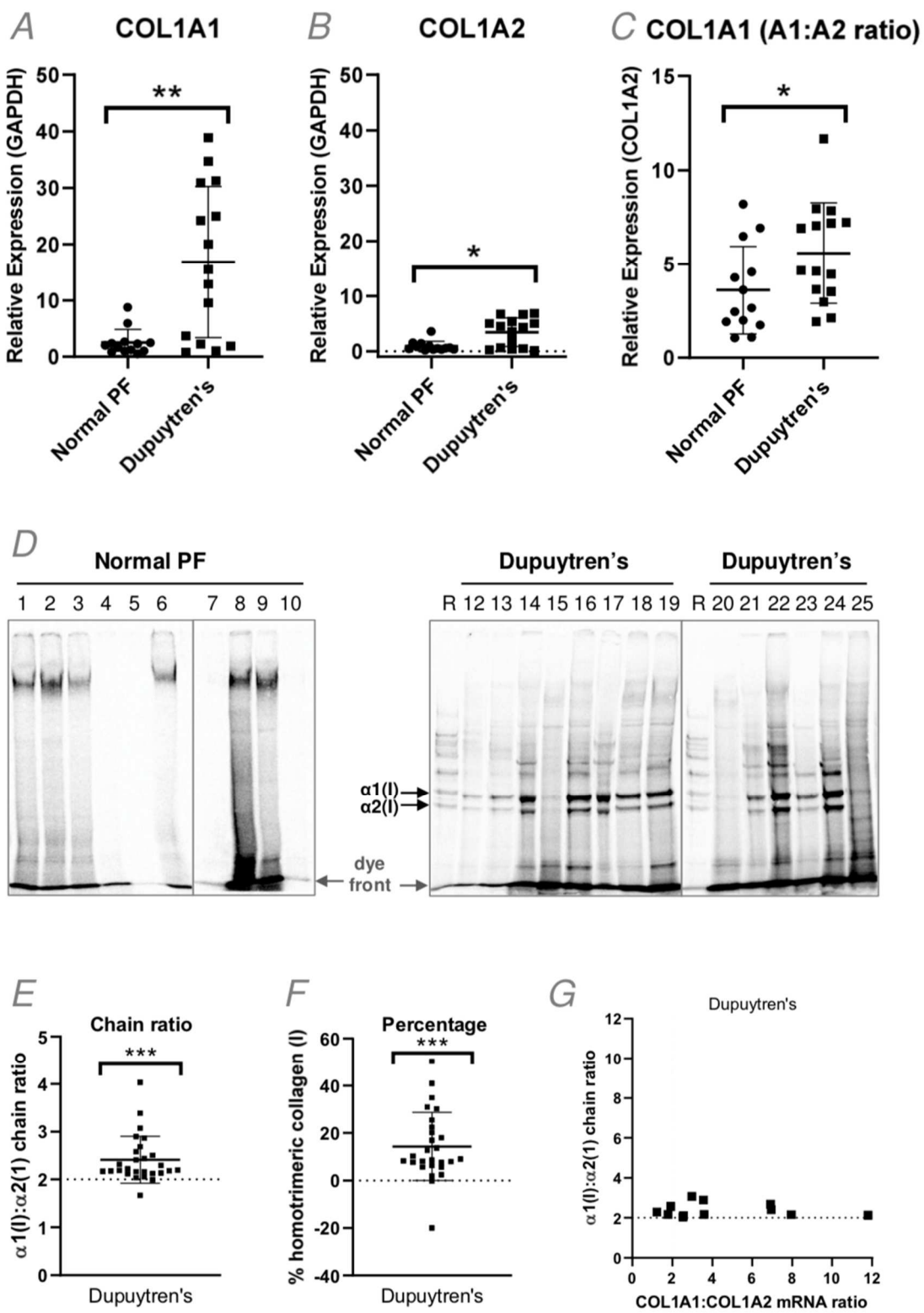

Figure 1: Synthesis of type I collagen homotrimer by Dupuytren's tissue. A-C: Analysis of COL1A1 (A), COL1A2 (B) and COL1A1:COL1A2 (C) gene expression by qRT-PCR in normal PF (n=13) and Dupuytren's tissue samples (n=15). D: Representative delayed reduction 6% SDS-Page gels of normal PF (D) and Dupuytren's (E) tissue extracts after pulse-chase labelling with [^{14}C]proline. E-F: The relative amounts of the labelled α1(I) and α2(I) chains in Dupuytren's (n=27) samples were quantified by densitometry and expressed as an α1(I):α2(I) chain ratio (E) or converted to a percentage of homotrimeric type I collagen (I) (F). The α1(I):α2(I) chain ratio was plotted against the COL1A1:COL1A2 mRNA ratio for Dupuytren's samples (n=12) for which both data types were available (G). * p<0.05, ** p<0.01 and *** p<0.001.

Demographic factors are not associated with greater collagen (I) homotrimer synthesis

To determine if particular demographics factors were associated with an increased proportion of homotrimeric collagen (I), a PCA was carried out (Fig. 2). Samples producing lower (<10%), medium (10-25%) or higher (>25%) percentages of homotrimeric collagen (I) were not grouped based on demographics factors (Fig. 2A). Demographic loading (Fig. 2B) had a minimal effect on principal component scores. To determine whether disease stage influences collagen (I) homotrimer synthesis, the PCA was repeated on samples with paired disease stage, which also showed only a weak effect (Fig. 2C-D).

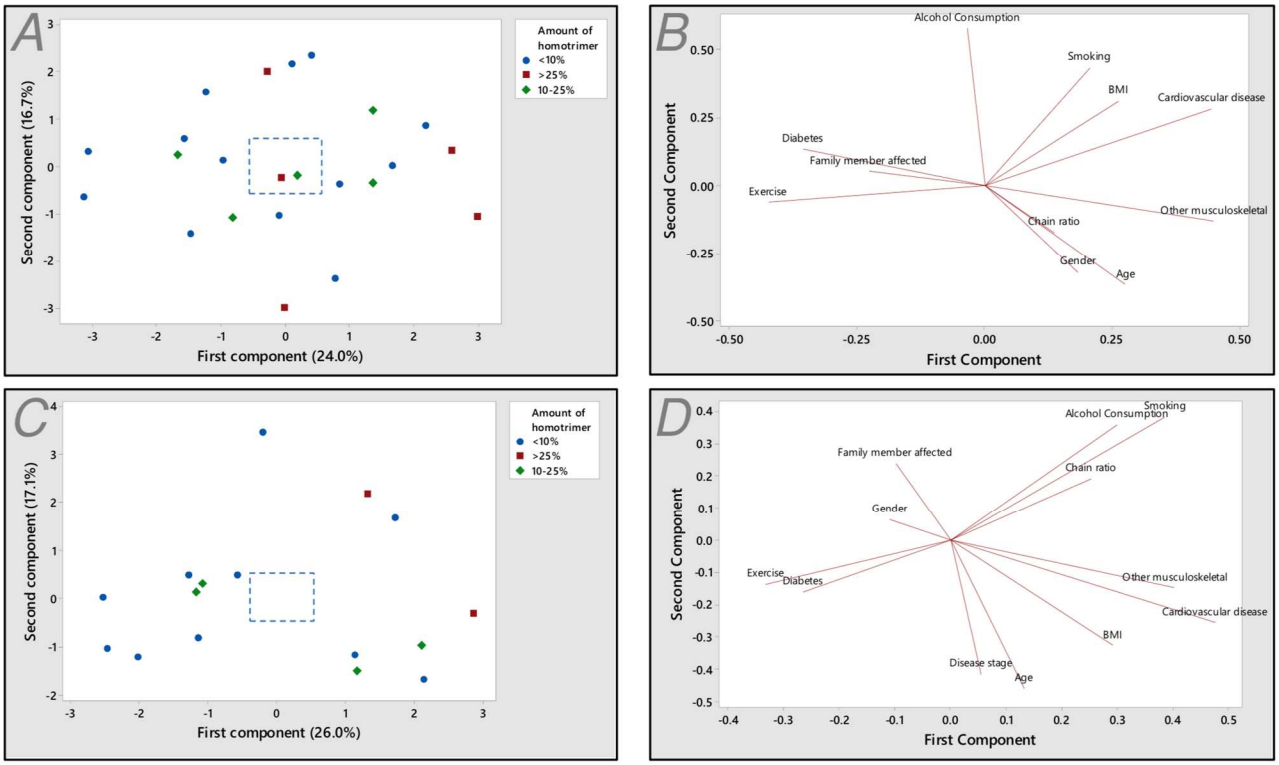

Figure 2: Principal components analysis of the relationship between demographic factors and the proportion of homotrimeric collagen. A: Score plot grouped by lower (<10%), medium (10-25%) and higher (>25%) percentages of collagen (I) homotrimer (n=23). The box indicates the relative scale on the loading plot (B). C-D: Score plot (C) and loading plot (D) for a patient sub-set with disease stage information (n=16).

Active type I collagen synthesis in diseased, ruptured or foetal, but not healthy adult fibrous connective tissue

No radiolabelled normal PF samples were found to synthesise detectable amounts of type I collagen in explant culture, but a high molecular weight band was noted in 10 of the 22 labelled normal PF samples (examples shown in Fig. 1D). Under reducing conditions, a single band migrating similarly to the α2(I) chain was noted in normal PF samples and one between the α1(I) and α2(I) chain in some Dupuytren's samples (#s 12, 14 and 19) (Fig. 3A). The identity of the labelled proteins in these bands are unknown but are expected to be collagenous given the incorporation of labelled proline.

We considered that the age and normal status of the normal PF samples may preclude detectable levels of new type I collagen synthesis. Model non-fibrotic fibrous connective tissues were therefore studied. Analysis of canine cranial cruciate ligament (CCL) allowed a comparison between healthy fibrous tissue, and that ruptured due to degenerative disease, whilst analysis of equine superficial digital flexor tendon (SDFT) facilitated a comparison across ages: foetal, young, adult and old. The relative expression of both COL1A1 (Fig. 3B) and COL1A2 (Fig. 3C) was significantly increased in ruptured canine cranial cruciate ligament as compared to healthy samples. The expression of COL1A1 relative to COL1A2 was higher in ruptured ligament (Fig. 3D), although the ratio did not exceed 1.5. Ruptured ligament produced newly-synthesised type I collagen whilst under reducing conditions healthy ligament produced a single band migrating between the α1(I) and the α2(I) chain (Fig. 3E). Foetal SDFT produced nascent type I collagen as expected, whilst all post-natal SDFT samples did not; instead producing a band co-migrating with α2(I) (similar to human normal PF), a higher molecular weight band co-migrating with pCα2(I) and often a band migrating between proα1(I) and pCα1(I).

Over page:

Figure 3: Type I collagen and proline-rich protein synthesis in tendon and ligament explants. A: Representative 4% SDS-Page gels of reduced normal PF and Dupuytren's tissue extracts after pulse-chase labelling with [^{14}C]proline. Sample numbers relate to those shown in Figure 1D. B-D: Analysis of COL1A1 (B), COL1A2 (C) and COL1A1:COL1A2 (D) gene expression by qRT-PCR in healthy (n=9) and ruptured (n=14) canine cranial cruciate ligament samples. E: Representative 4% SDS-Page gel of reduced healthy and ruptured canine cranial cruciate ligament extracts after pulse-chase labelling with [^{14}C]proline. F: Representative 4% SDS-Page gel of equine superficial digital flexor tendon (SDFT) extracts at different ages after pulse-chase labelling with [^{14}C]proline. G-H: Analysis of COL1A1 and COL1A2 (G) and COL1A1:COL1A2 (H) gene expression by qRT-PCR in equine superficial digital flexor tendon (SDFT) at various ages. Note horses have an average 25-30 year lifespan, with 20 years being equivalent to approximately 60 human years.

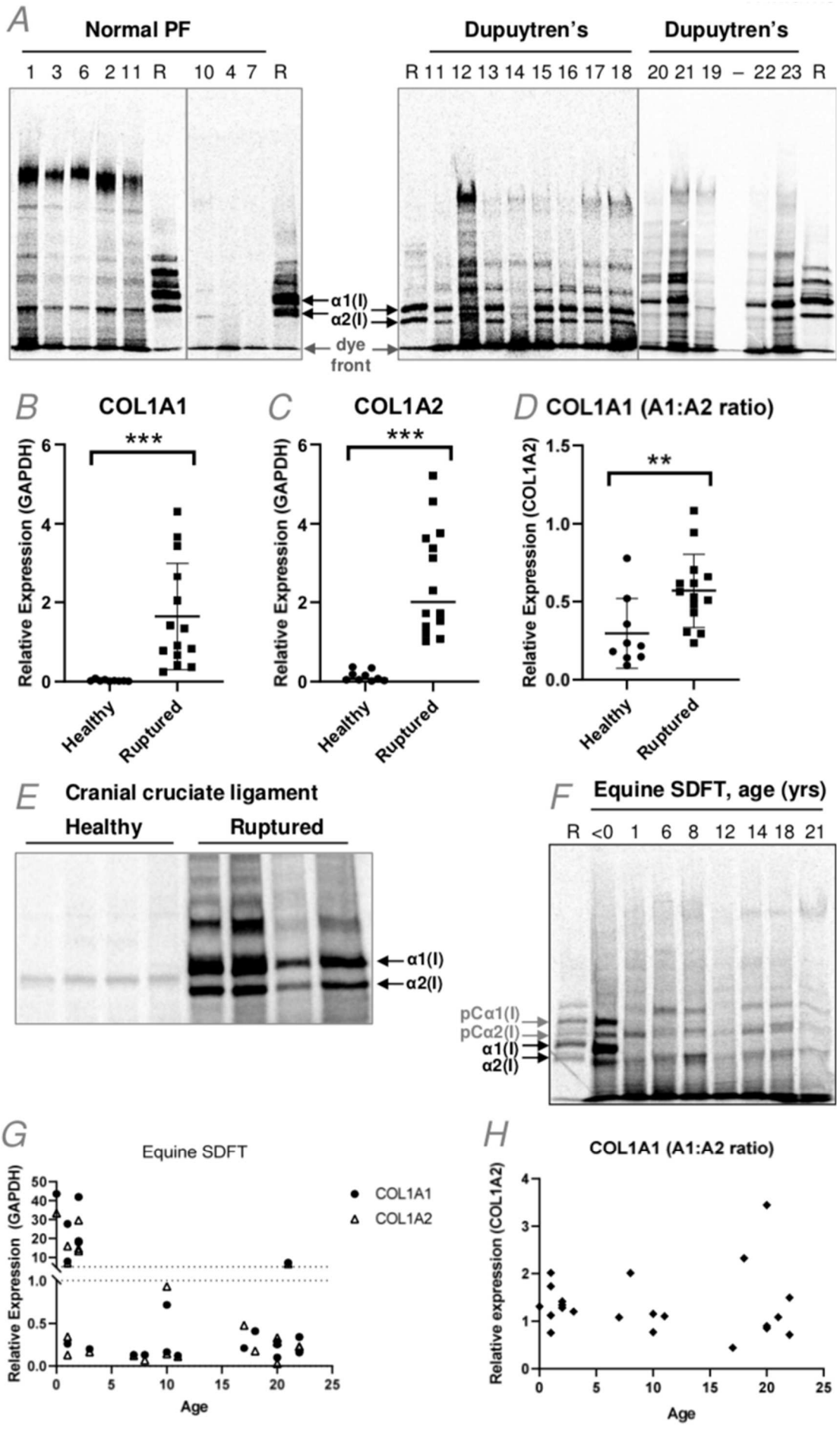

353

Active synthesis of matrisomal proteins by Dupuytren's tissue

Samples were allocated for the proteomics workflow prior to final confirmation of patient age and gender information on the day of surgery. Datasets were then selected for inclusion to minimise key differences between groups and facilitate statistical analysis. Table 2 shows the age and gender distribution of the samples included in the proteomics analysis.

Table 2: Age and gender distribution of samples analysed by proteomics. Disease stage information (Tubiana) for Dupuytren's samples is included.

	Normal palmar fascia		Dupuytren's		
	Age	**Gender**	**Age**	**Gender**	**Disease stage**
	48	M	49	M	4
	51	F	62	F	2
	58	M	75	M	4
	68	M	76	M	2
	89	F			
Mean	**62.8**		**65.5**		
SD	**16.5**		**12.7**		

There was no significant difference in the age of samples in each group ($p=0.796$). A Bayesian analysis indicated substantial evidence that there was no difference in age between the groups ($B=0.17$).

To identify newly synthesized proteins in Dupuytren's nodule, cord and normal PF tissue, tissue explants were labelled with heavy lysine, and both tissue extracts and media analysed for new protein synthesis (heavy peptide content) and turnover (total peptide content) as described (Lee et al., 2019). No labelling was detected above background in tissue extracts, although labelled matrisomal proteins collagen (I) (Fig 4A-D), fibronectin (Fig 4E-F), IGFBP7 (Fig. 4G-H), MMP3 (Fig. 5A-B), MMP2 (Fig. 5C-D) and TIMP2 (Fig. 5E-F) were detected in media. Fibronectin and IGFBP7 are ECM Glycoproteins, whereas MMP3, MMP2 and TIMP2 are ECM Regulators. Of these, labelled collagen (I), MMP3 and TIMP2 were significantly higher in media from either Dupuytren's nodule or cord, than from normal PF. Fibronectin and MMP2 showed unspecified differences between sample types. Peptide quantity was not significantly reduced in normal PF media, (although was notably lower in Dupuytren's nodule or cord for MMP3 and TIMP2,) indicating that results were not skewed by explant size. Notably the relative isotope abundance for fibronectin was particularly low (<5%) and IGFBP7 was actively synthesized similarly by normal PF, Dupuytren's nodule and cord.

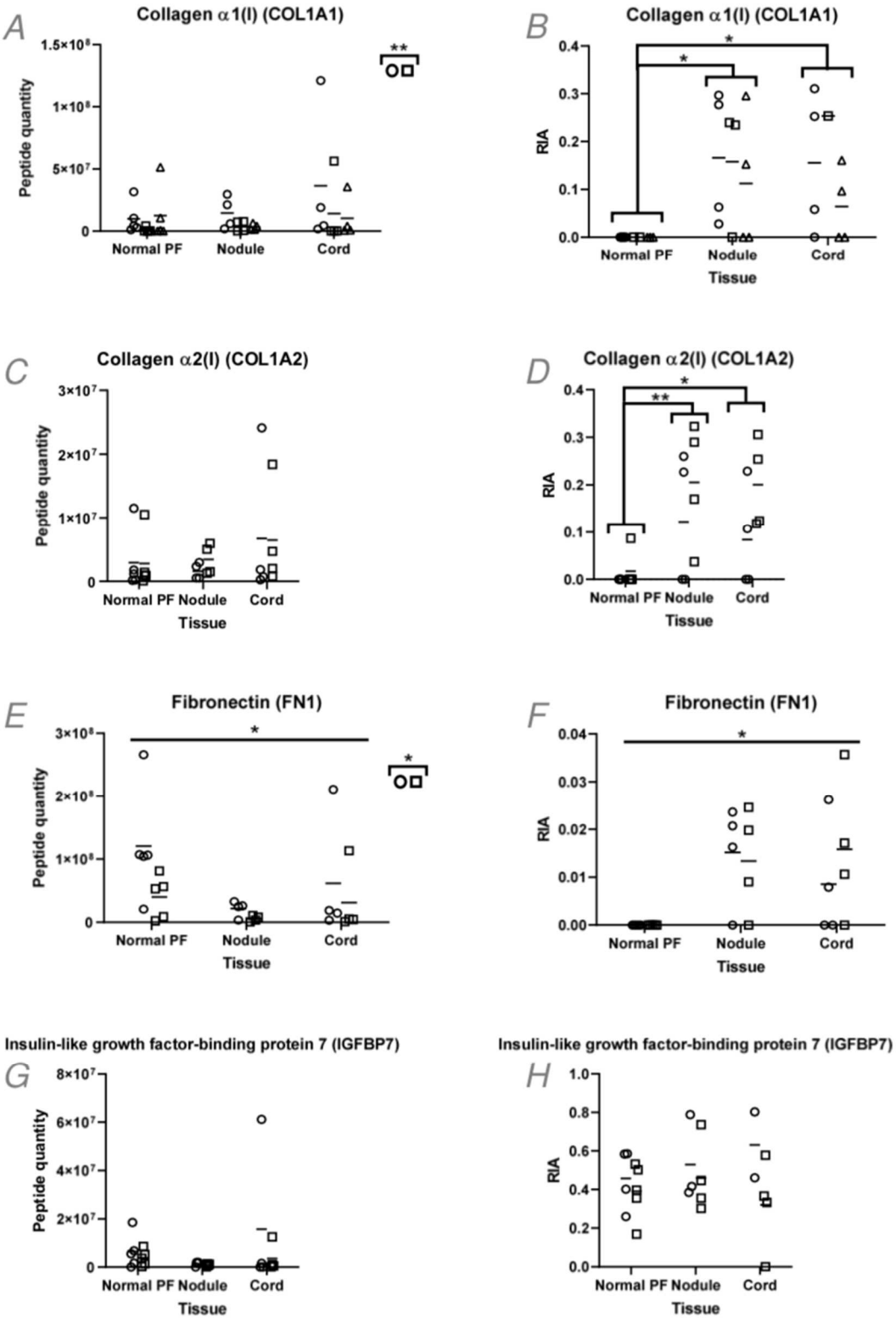

Figure 4: Labelled core matrisomal proteins in media of normal palmar fascia (PF) and Dupuytren's tissue explants. ECM proteins labelled with ^{13}C lysine were identified using MASCOT and extracted ion chromatograms were analysed using Xcalibur. Heavy (H) and light (L) peaks were identified for each labelled peptide and the area under the peak recorded. Total peptide quantity (H+L) normalised to equivalent tissue weight analysed (A, C, E, G) and relative isotope abundance (RIA) (H/(L+H)) (B, D, F, H) are shown. A&B: collagen α1(I), C&D: collagen α2(I), E&F: fibronectin, G&H: insulin-like growth factor-binding protein. Different symbols represent different peptides and the bar represents the mean. * $p<0.05$, ** $p<0.01$ and *** $p<0.001$.

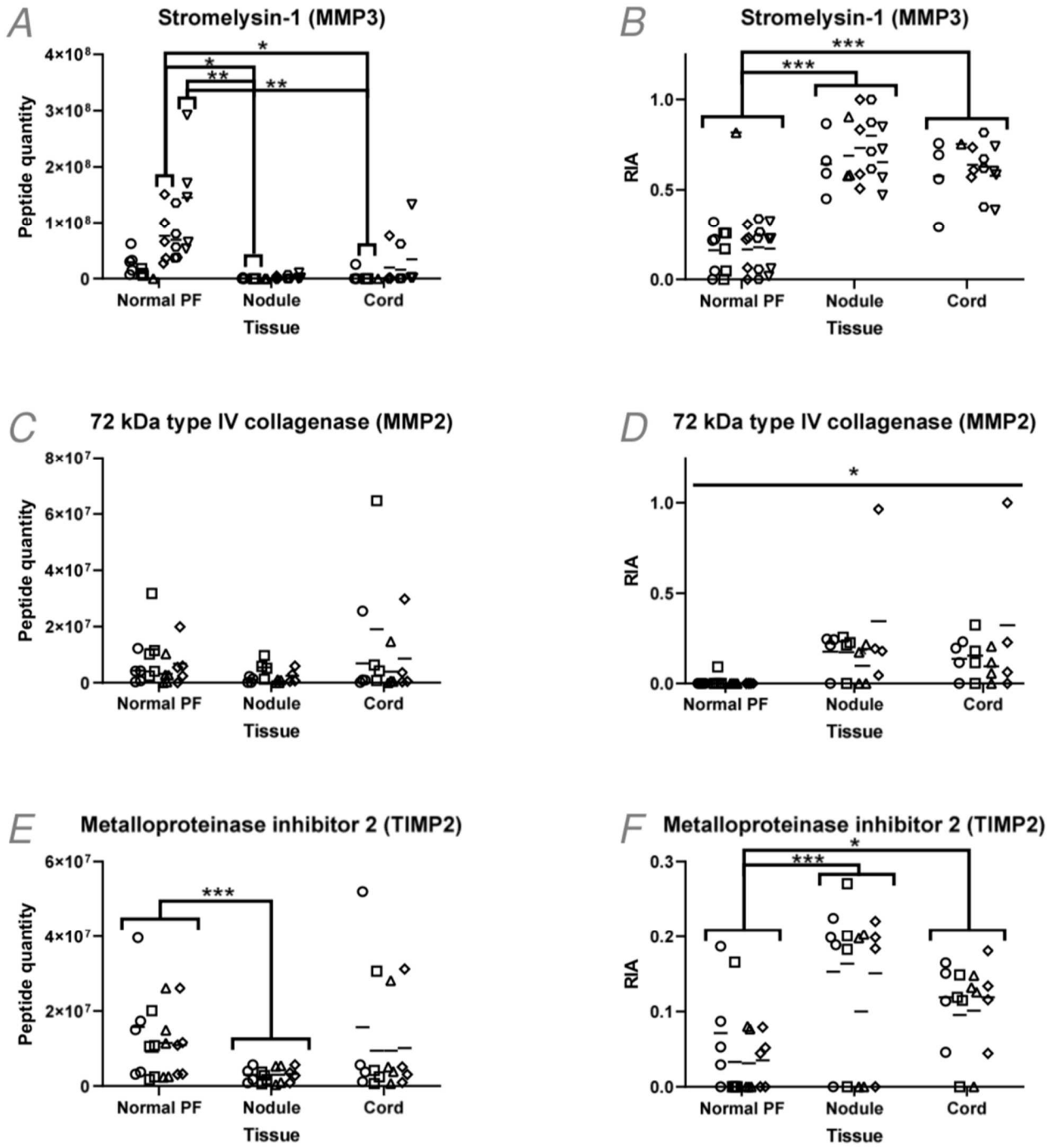

Figure 5: Labelled ECM Regulators in media of normal palmar fascia (PF) and Dupuytren's tissue explants. Enzymes and protein inhibitors labelled with ^{13}C lysine were identified using MASCOT and extracted ion chromatograms were analysed using Xcalibur. Heavy (H) and light (L) peaks were identified for each labelled peptide and the area under the peak recorded. Total peptide quantity (H+L) normalised to equivalent tissue weight analysed (A, C, E) and relative isotope abundance (RIA) (H/(L+H)) (B, D, F,) are shown. A&B: matrix metalloproteinase 3, C&D: matrix metalloproteinase 2, E&F: tissue inhibitor of metalloproteinase 2. Different symbols represent different peptides and the bar represents the mean. * $p<0.05$, ** $p<0.01$ and *** $p<0.001$.

405 **TGFβ is implicated in the matrisomal profile of Dupuytren's tissue**

406 Label-free analysis of media and principal component analysis indicated that normal PF grouped separately
407 from Dupuytren's media, but that nodule and cord did not cluster into discrete groups (Supplementary Fig.
408 S1A). Matrisomal proteins comprised 31% of those proteins enriched in Dupuytren's media and TGFβ was
409 identified as the top potential upstream regulator using Ingenuity Pathway Analysis (IPA). Of those proteins
410 predicted to be regulated by TGFβ, 46% were matrisomal proteins (Supplementary Fig. S1B) and primarily
411 ECM glycoproteins (Supplementary Fig. S1C). STRING protein-protein network analysis highlighted the few
412 proteins enriched in normal PF media, including notably MMP3 (Supplementary Fig. S2A) and the well-
413 connected cluster of matrisomal proteins enriched in Dupuytren's media (Supplementary Fig. S2B).
414 Our previous proteomic analysis of tendon and ligament tissue included a chondroitinase ABC
415 treatment step to remove highly negatively charged glycosaminoglycans (Kharaz et al., 2016), as did earlier
416 studies (Peffers et al., 2014; Wilson et al., 2010) and the work on which we based our guanidine/rapigest
417 extraction methodology (Ashraf Kharaz et al., 2017). Removal of large negatively charged
418 glycosaminoglycans could improve proteoglycan identification by improving protein digestion and peptide
419 fractionation, but chondroitinase digestion also generates a supernatant to which some proteins could be
420 lost. During tissue preparation in the present study the chondroitinase ABC treatment step was either
421 omitted, or included and the chondroitinase supernatant reserved, and protein abundance compared
422 between untreated, treated and supernatant. Heatmaps indicated some loss of proteins into the
423 chondroitinase ABC supernatant, with increased abundance of several proteins in the supernatant of
424 normal PF and Dupuytren's cord samples (Supplementary Fig. S3). Whilst arguably chondroitinase ABC
425 treatment increased the detection of some proteins in Dupuytren's nodule and cord, it generally decreased
426 detection in normal PF, and approximately equal numbers of proteins showed decreased versus increased
427 abundance with chondroitinase treatment in Dupuytren's cord. For normal PF and cord there was evidence
428 of some loss of proteins to the chondroitinase supernatant. Analysis was therefore performed on samples
429 without the chondroitinase treatment step.
430 Label-free and PCA analysis of tissue processed without chondroitinase treatment again indicated
431 that nodule and cord samples could not be distinguished on the basis of protein abundance (Fig. 6A). In the
432 PCA one cord sample overlapped with the normal PF group. There was no overt difference in the
433 appearance of the PCA plot for untreated and chondroitinase-treated samples (not shown). Matrisomal
434 proteins again comprised 31% of those proteins enriched in Dupuytren's tissue and TGFβ was identified as
435 the top potential upstream regulator using IPA. Of those proteins more abundant in Dupuytren's tissue and
436 predicted to be regulated by TGFβ, 46% were matrisomal proteins (Fig. 6B) and were a mixture of
437 collagens, ECM glycoproteins, ECM regulators and other matrisomal categories (Fig. 6C).
438
439

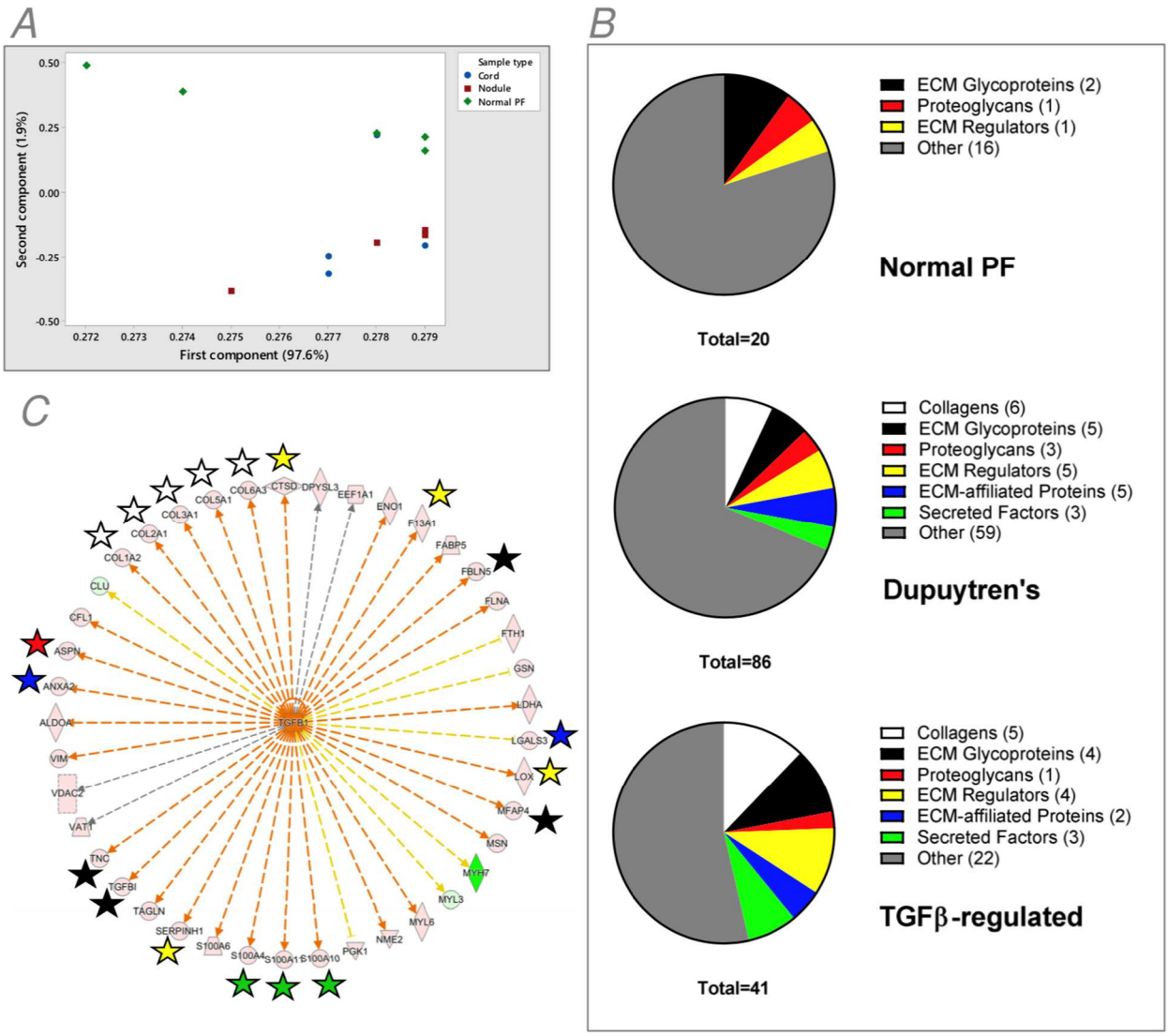

Figure 6. Label-free proteomics analysis of normal palmar fascia (PF) and Dupuytren's explant tissue. A: Principal component analysis score plot grouped by tissue type. B: Enriched proteins in normal PF tissue, Dupuytren's tissue and those in Dupuytren's tissue predicted to be regulated by TGFβ, subdivided based on matrisomal classification. C: Ingenuity Pathway Analysis (IPA) diagram highlighting matrisomal proteins within those predicted to be regulated by TGFβ. Red; increased abundance, green; decreased abundance, orange; predicted to lead to activation, blue; predicted to lead to inhibition, yellow; findings inconsistent with state of downstream molecule, grey; effect not predicted. Matrisomal proteins are indicated with a star (collagens; white, ECM Glycoproteins; black, ECM-affiliated Proteins; blue, Proteoglycans; red, ECM Regulators; yellow, Secreted Factors; green)

STRING protein-protein network analysis highlighted the few proteins enriched in normal PF tissue, grouped into three small clusters (Fig. 7A), and the well-connected cluster of matrisomal proteins more abundant in Dupuytren's tissue (Fig. 7B). For normal PF tissue, the top reactome pathways were amyloid fiber formation (FDR 0.0051), formation of the cornified envelope (FDR 0.0106), striated muscle contraction (FDR 0.0125), regulation of complement cascade (FDR 0.0172), and retinoid metabolism and transport (FDR 0.0172). For Dupuytren's tissue, the top reactome pathways were immune system (FDR 1.69e-16), neutrophil degranulation (FDR 2.76e-14), extracellular matrix organization (FDR 2.25e-13), innate immune system (1.46e-11), and collagen formation (4.48e-11).

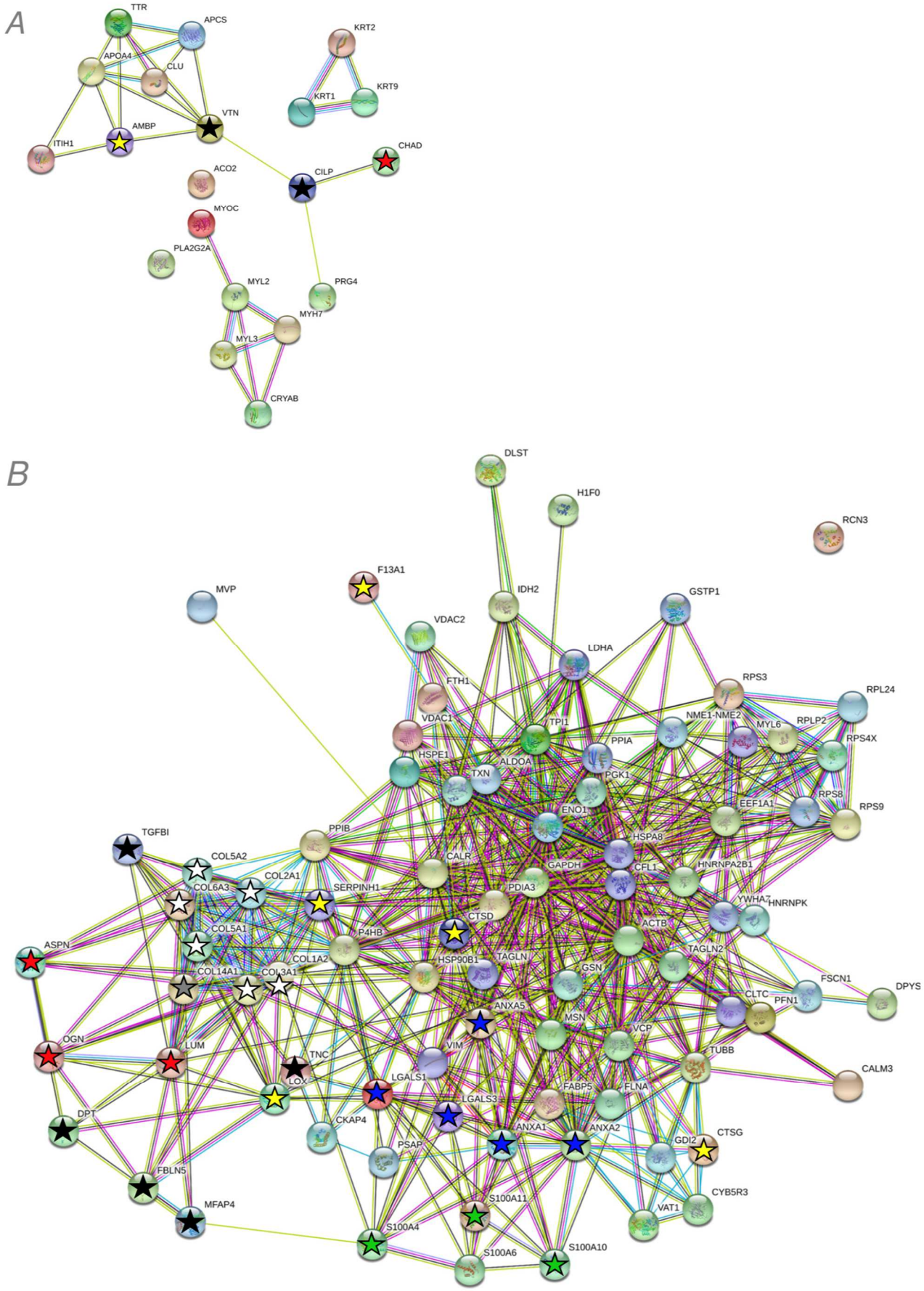

461

Figure 7. STRING interaction networks for normal palmar fascia (PF) and Dupuytren's explant tissue processed without chondroitinase ABC treatment. A: Interaction network for proteins enriched in normal PF explant tissue. B: Interaction network for proteins enriched in Dupuytren's explant tissue.

The large skew in protein enrichment in Dupuytren's tissue, when normalising by wet weight of tissue, indicated that proteins may be more readily extracted from Dupuytren's than normal PF. Performing the label-free analysis with a normalisation to total ion chromatogram resulted in a more even distribution between tissue types (Supplementary Fig. S4). For normal PF tissue, the top reactome pathways were integrin cell surface interactions (FDR 2.22e-09), collagen chain trimerization (FDR 5.07e-08), extracellular matrix organization (FDR 5.07e-08), assembly of collagen fibrils and other multimeric structures (FDR 1.87e-07), and collagen degradation (FDR 2.14e-07). For Dupuytren's tissue, the top reactome pathways were neutrophil degranulation (FDR 2.74e-09), immune system (FDR 3.95e-09), axon guidance (FDR 8.93e-07), innate immune system (8.93e-07), and influenza life cycle (9.84e-07).

Given the higher protein synthesis of MMP3 by Dupuytren's nodule and cord when compared to normal PF (Fig. 5), we considered whether there were differences in peptides indicative of protein degradation between tissues. Neopeptides were identified and filtered by occurrence in at least 3 samples of normal PF explant media (Table 3), Dupuytren's explant media (Table 4), normal PF tissue (Table 5) or Dupuytren's tissue (Table 6). There were several neopeptides for CILP, TNXB, MYOC in at least 3 normal PF media and tissue samples, with MYH7 and MYOC neopeptides being present in at least 3 normal PF tissue samples but absent from Dupuytren's tissue. Two periostin neopeptides were present in at least 3 Dupuytren's nodule and cord media samples, but not in normal PF media, and three periostin neopeptides were present in at least 3 Dupuytren's nodule and cord tissue samples, but there was only one periostin neopeptide in one normal PF sample.

508 **Table 3: Neopeptides unique to normal palmar fascia (PF) media from ≥3 samples.** Proteins in bold have
509 neopeptides only in normal PF media. Brackets indicate the total number samples in which neopeptides
510 were identified of 5 samples total. The total number of neopeptide sequences are for that protein across all
511 tissue samples, hence not all unique.

Protein (abbreviation)	Number of neopeptides unique to normal PF media (in how many samples)	Total number of neopeptide sequences
Cartilage intermediate layer protein 1 (CILP)	7 (2 in 4; 5 in 3)	127
Myocilin (MYOC)	6 (3 in 4; 3 in 3)	128
Tenascin-X (TNXB)	6 (2 in 4; 4 in 3)	830
Neuroblast differentiation-associated protein AHNAK (AHNAK)	4 (3)	622
Procollagen C-endopeptidase enhancer 2 (PCOLCE2)	2 (1 in 4; 1 in 3)	7
Alpha-crystallin B chain (CRYAB)	**2 (4)**	**10**
Chondroadherin (CHAD)	**2 (1 in 5; 1 in 4)**	**10**
Histone H1.4 (HIST1H1E)	2 (1 in 4; 1 in 3)	15
Proteoglycan 4 (PRG4)	2 (1 in 4; 1 in 3)	20
Biglycan (BGN)	2 (1 in 4; 1 in 3)	28
Matrilin-2 (MATN2)	2 (1 in 4; 1 in 3)	31
Spectrin alpha chain, non-erythrocytic 1 (SPTAN1)	2 (3)	107
Collagen alpha-3(VI) chain (COL6A3)	2 (3)	313
Fibronectin (FN1)	2 (3)	594
Ezrin (EZR)	**1 (3)**	**3**
Lipopolysaccharide-binding protein (LBP)	**1 (3)**	**3**
Ras-related protein R-Ras (RRAS)	**1 (3)**	**3**
Chondroitin sulfate proteoglycan 4 (CSPG4)	**1 (3)**	**5**
Creatine kinase M-type (CKM)	**1 (3)**	**6**
PDZ and LIM domain protein 5 (PDLIM5)	1 (4)	7
Ras-related protein Rap-1b (RAP1B)	**1 (4)**	**10**
Actin, aortic smooth muscle (ACTA2)	**1 (3)**	**12**
Complement factor H-related protein 1 (CFHR1)	1(3)	17
Complement C1q subcomponent subunit B (C1QB)	1 (3)	18
Clathrin light chain B (CLTB)	1 (4)	21
Protein AMBP (AMBP)	1 (3)	22
Lactadherin (MFGE8)	1 (4)	23
Fibrillin-1 (FBN1)	1 (3)	27
Tubulin alpha-1C chain (TUBA1C)	1 (3)	32
Moesin (MSN)	1 (3)	33
Clusterin (CLU)	1 (4)	34
Extracellular superoxide dismutase [Cu-Zn] (SOD3)	1 (3)	43
Spectrin beta chain, non-erythrocytic 1 (SPTBN1)	1 (4)	47
Stromelysin-1 (MMP3)	1 (3)	51
Decorin (DCN)	1 (3)	64

Procollagen C-endopeptidase enhancer 1 (PCOLCE)	**1 (3)**	**105**
Fibulin-1 (FBLN1)	1 (3)	120
Plectin (PLEC)	1 (3)	202
Complement C3 (C3)	1 (3)	205
Vimentin (VIM)	1 (3)	351

Table 4: Neopeptides unique to Dupuytren's media from ≥3 nodule and cord samples. Proteins in bold have neopeptides in both Dupuytren's cord and nodule media, but not in normal palmar fascia media. Brackets indicate the total number samples in which neopeptides were identified of 4 samples total. The total number of neopeptide sequences are for that protein across all media samples, hence not all unique.

Protein (abbreviation)	Number of neopeptides unique to Dupuytren's media (in how many nodule, cord samples)	Total number of neopeptide sequences
Adipocyte enhancer-binding protein 1 (AEBP1)	3 (1 in 4, 4; 2 in 3, 3)	77
Periostin (POSTN)	**2 (4, 3)**	**57**
Collagen alpha-1(XIV) chain (COL14A1)	2 (3, 4)	134
Urotensin-2 (UTS2)	**1 (3, 3)**	**6**
Adenylyl cyclase-associated protein 1 (CAP1)	**1 (3, 3)**	**8**
Phosphatidylethanolamine-binding protein 1 (PEBP1)	**1 (3, 4)**	**10**
Ribonuclease inhibitor (RNH1)	1 (3, 3)	24
Serotransferrin (TF)	1 (4, 3)	26
Olfactomedin-like protein 3 (OLFML3)	1 (4, 4)	29
Profilin-1 (PFN1)	1 (3, 3)	30
Phosphoglycerate kinase 1 (PGK1)	1 (3, 4)	31
Endoplasmic reticulum chaperone BiP (HSPA5)	1 (3, 3)	39
Hemoglobin subunit beta (HBB)	1 (3, 4)	51
Galectin-1 (LGALS1)	1 (3, 3)	69
Immunoglobulin kappa constant (IGKC)	1 (3, 3)	96
Immunoglobulin heavy constant gamma 1 (IGHG1)	1 (3, 3)	100
Actin, cytoplasmic 1 (ACTB)	1 (3, 4)	108
Collagen alpha-3(VI) chain (COL6A3)	1 (4, 4)	313
Fibronectin (FN1)	1 (4, 3)	594

525 **Table 5: Neopeptides unique to ≥3 normal palmar fascia (PF) tissue samples.** Proteins in bold have
526 neopeptides only in normal PF tissue. Brackets indicate the total number samples in which neopeptides
527 were identified of 4 samples total. The total number of neopeptide sequences are for that protein across all
528 tissue samples, hence not all unique.

Protein (abbreviation)	Number of neopeptides unique to normal PF tissue (in how many samples)	Total number of neopeptide sequences
Cartilage intermediate layer protein 1 (CILP)	10 (6 in 4; 4 in 3)	65
Tenascin-X (TNXB)	8 (2 in 5; 1 in 4; 5 in 3)	187
Myosin-7 (MYH7)	**7 (4 in 3, 3 in 4)**	**93**
Myocilin (MYOC)	**6 (1 in 5; 1 in 4; 4 in 3)**	**27**
Keratin, type II cytoskeletal 2 epidermal (KRT2)	4 (3)	25
Keratin, type I cytoskeletal 10 (KRT10)	4 (3)	74
Fibronectin (FN1)	4 (1 in 5; 3 in 4)	166
Fibrillin-1 (FBN1)	4 (1 in 5; 1 in 4; 2 in 3)	205
Vitronectin (VTN)	3 (1 in 5; 1 in 4; 1 in 3)	19
Basement membrane-specific heparan sulfate proteoglycan core protein (HSPG2)	3 (1 in 4; 1 in 3)	64
Keratin, type II cytoskeletal 1 (KRT1)	3 (2 in 5; 1 in 3)	96
Collagen alpha-2(IV) chain (COL4A2)	2 (3)	8
Protein AMBP (AMBP)	2 (2)	18
Versican core protein (VCAN)	2 (3)	20
Keratin, type I cytoskeletal 9 (KRT9)	2 (1 in 4; 1 in 3)	57
Decorin (DCN)	2 (1 in 5; 1 in 3)	88
Thrombospondin-4 (THBS4)	2 (1 in 5; 1 in 3)	112
Collagen alpha-2(I) chain (COL1A2)	2 (1 in 5; 1 in 3)	178
Collagen alpha-1(IV) chain (COL4A1)	1 (3)	4
Phospholipase A2, membrane associated (PLA2G2A)	1 (3)	4
Alpha-crystallin B chain (CRYAB)	1 (3)	5
Fibulin-1 (FBLN1)	1 (3)	6
Myosin light chain 1/3, skeletal muscle isoform (MYL1)	**1 (4)**	**7**
Tubulin beta-2B chain (TUBB2B)	1 (3)	8
Histone H2B type 3-B (HIST3H2BB)	**1 (5)**	**9**
Lactadherin (MFGE8)	1 (3)	13
EMILIN-1 (EMILIN1)	1 (4)	15
Target of Nesh-SH3 (ABI3BP)	1 (3)	20
Clusterin (CLU)	1 (5)	25
ATP synthase subunit alpha, mitochondrial (ATP5F1A)	1 (4)	31
Fibromodulin (FMOD)	1 (4)	59
Serum albumin (ALB)	1 (4)	60
Collagen alpha-2(VI) chain (COL6A2)	1 (3)	130
Cartilage oligomeric matrix protein (COMP)	1(4)	145
Collagen alpha-1(VI) chain (COL6A1)	1 (4)	149
Collagen alpha-1(I) chain (COL1A1)	1 (3)	188

Collagen alpha-1(XII) chain (COL12A1)	1 (4)	326
Collagen alpha-3(VI) chain (COL6A3)	1 (3)	607

Table 6: Neopeptides unique to ≥3 Dupuytren's nodule and cord samples tissue samples. Brackets indicate the total number samples in which neopeptides were identified of 4 samples total. The total number of neopeptide sequences are for that protein across all tissue samples, hence not all unique. * Only one POSTN neopeptide was identified in one normal palmar fascia tissue sample.

Protein (abbreviation)	Number of neopeptides unique to Dupuytren's tissue (in how many nodule, cord samples)	Total number of neopeptides for the protein
Periostin (POSTN)	3 (3, 4)	80*
Collagen alpha-1(XIV) chain (COL14A1)	2 (1 in 4, 3; 1 in 3, 3)	126
Annexin A5 (ANXA5)	1 (3)	42
Collagen alpha-1(I) chain (COL1A1)	1 (4, 3)	188
Collagen alpha-3(VI) chain (COL6A3)	1 (3, 4)	607

Discussion

In this study, we showed increased COL1A1 and COL1A2 mRNA as well as an increased COL1A1:COL1A2 mRNA ratio in Dupuytren's tissue as compared to normal PF (Fig. 1 A-C). The results presented are in accordance with previous studies which showed increased COL1A1 mRNA in Dupuytren's tissue compared to unaffected transverse ligament of the palmar aponeurosis (Ten Dam et al., 2016) and increased COL1A1 but not COL1A2 mRNA in Dupuytren's tissue, as compared to shoulder capsule (Kilian et al., 2007). In the present study, we did not distinguish between nodule and cord for RNA analysis, although a prior study found both COL1A1 and COL1A2 mRNA was higher in nodule as compared to cord, despite lower collagen (I) protein being present in nodule (van Beuge et al., 2016).

One previous study indicated the presence of collagen (I) homotrimer in Dupuytren's tissue with an increase from 5% in normal PF, to 9% in Dupuytren's utilising pooled samples (Ehrlich et al., 1982). Utilising metabolic labelling with ^{14}C proline, we found a consistent increase in the α1(I):α2(I) polypeptide chain ratio for newly synthesised collagen in Dupuytren's tissue samples, but noted a skewed distribution with some samples showing a particularly high α1(I):α2(I) chain ratio (Fig. 1 ~~EF~~). We hypothesised that individual variation or samples analysed at different stages of disease progression may be responsible for the relative proportion of newly synthesised collagen however, no association with demographics data or disease stage was observerd (Fig. 2). It is likely that the sample size is too low to identify factors or interactions that may direct high collagen (I) homotrimer synthesis or that the granularity of the demographics data is insufficient. The mean percentage of homotrimeric collagen is higher than that reported by Ehrlich et. al, although there is a cluster of several samples apparently synthesizing collagen (I) homotrimer to a similar extent, at around 10%. Notably our study also provides a snapshot of collagen (I) homotrimer synthesis whereas Ehrlich et. al. analysed accumulated homotrimeric collagen (I).

We noted an absence of detectable collagen (I) protein synthesis in normal PF by radiolabelling (Fig. 1D), and obtained similar results for healthy canine cranial cruciate ligament and post-natal equine

superficial digital flexor tendon. This indicated to us that the collagen (I) synthesis detected in Dupuytren's and ruptured cruciate ligament explants is not due to an acute injury response to dissection. In ruptured canine cranial cruciate ligament (CCL), expression of COL1A1 and COL1A2 mRNA was increased (Fig. 3 A-B). A previous study in canine CCL indicated a significant increase in COL1A2 mRNA, but not of COL1A1 in ruptured ligaments (Clements et al., 2008), whilst COL1A1 mRNA was found to be increased in ruptured human anterior cruciate ligament by in situ hybridization (Fukui et al., 2001). In the present study, the COL1A1:COL1A2 ratio was significantly higher in ruptured canine CCLs but the ratio did not exceed 2 and collagen (I) homotrimer synthesis was not apparent (Fig. 3E). Gene expression of COL1A1 and COL1A2 in equine SDFT reduced dramatically after 2 years of age (Fig. 3G) and collagen (I) protein synthesis was only detected in fetal tendon (Fig. 3F), consistent with the known high level collagen (I) expression during embryonic tendon development (Robbins and Vogel, 1994). No age-related changes in the COL1A1:COL1A2 mRNA ratio were observed in equine SDFT.

Despite a lack of collagen (I) protein synthesis, we noted labelled bands in normal PF (Fig. 3A), canine CCL (Fig. 3E), and SDFT (Fig. 3F) tissue extracts. Attempts to identify the labelled proteins using ^{13}C proline labelling, band excision and mass spectrometry, or by Western blotting to candidate collagens were unfortunately, not informative. However, given the incorporation of ^{14}C proline, we expect that these proteins are collagenous in nature or proline-rich. Metabolic labelling with ^{13}C lysine was informative as to nascent proteins in the secretome of normal PF and Dupuytren's tissue explants. Labelled peptides for collagen α1(I) and α2(I) in Dupuytren's samples confirmed collagen (I) synthesis with up to around 30% of these peptides in the secretome being labelled (Fig. 4 A-D). The proportion of labelled fibronectin peptides was much lower, at less than 4% (Fig. 4F)., implying that much of the fibronectin in the secretome leached from the tissue.

The presence of labelled IGBP7 peptides was an unexpected finding, being synthesized by normal PF as well as by Dupuytren's tissue (Fig. 4H). IGFBP7 has not been previously identified in tendon or ligament to our knowledge, although we previously identified IGFBP6 as a cross-species tendon marker (Turlo et al., 2019). IGFBP7 binds the IGF1 receptor to block activation by IFGs (Evdokimova et al., 2012) and has been reported to act as a tumour suppressor (Akiel et al., 2017). A role for IGFBP7 in promoting osteogenic differentiation via Wnt/β-catenin (Zhang et al., 2018) and as a negative regulator of osteoclastogenesis has been reported (Ye et al., 2020). Hence IGFBP7 may play an unidentified role in tendon/ligament biology.

Labelled peptides for MMP3 were present at higher levels in Dupuytren's nodule and cord media than in normal PF media (Fig. 5A). Labelled MMP3 peptides showed the highest ^{13}C lysine label incorporation, with up to 100% of these peptides being labelled (Fig. 5B), whilst MMP3 was more abundant in normal PF media (Fig. S2A). Hence, MMP3 is actively synthesised by Dupuytren's tissue but may have leached out of the normal PF explant into the media during labelling. MMP3 gene expression was previously shown to be lower in Dupuytren's nodule than cord; and gene expression lower in both nodule and cord regions than in normal PF from carpal tunnel patients (Johnston et al., 2007). Hence post-transcriptional mechanisms or alterations during explant culture may be responsible for the presence of newly synthesized MMP3 in Dupuytren's media. To our knowledge, no study has previously implicated MMP3 in Dupuytren's disease, but a study utilising similar methodology for the secretome of cultured cancer-associated myofibroblasts identified MMP1, MMP2 and MMP3 as rapidly incorporating heavy lysine label (Hammond et al., 2018).

Labelled peptides for MMP2 showed unspecified differences between samples but appeared to be more abundant in nodule and cord (Fig. 5D). MMP2 was more abundant in Dupuytren's media by label-free quantification (Fig. S2B), whilst MMP2 gene expression was previously shown to be higher in cord than nodule, with both higher than control tissue (Johnston et al., 2007) and to correlate with disease

recurrence (Johnston et al., 2008). Increased MMP2 activation, as detected by zymography, was also previously observed in Dupuytren's as compared to palmar fascia from carpal tunnel patients (Augoff et al., 2006). MMP2 has been shown to facilitate fibroblast-mediated collagen gel contraction (Wilkinson et al., 2012) and hence may play a role in disease progression.

Labelled peptides for TIMP2 were present at higher levels in Dupuytren's nodule and cord than in normal PF media (Fig. 5F) and TIMP2 itself was more abundant in Dupuytren's media (Fig. S2B). Gene expression of TIMP2 was previously shown to be lower in Dupuytren's nodule than cord or control tissue (Johnston et al., 2007). Increased MMP2 and TIMP2 mRNA but a lower MMP2:TIMP2 mRNA ratio has been demonstrated in Dupuytren's tissue (Ratajczak-Wielgomas et al., 2012). Another study also showed that Dupuytren's patients had a lower serum MMP:TIMP ratio than carpal tunnel patient controls (where MMPs represented a combined measure of MMP1, MMP2 and MMP9, and TIMPs represented a combined measure of TIMP1 and TIMP2) (Ulrich et al., 2003). A lower ratio was also observed in those patients with active as compared to inactive disease. TIMP2 is an effective inhibitor of MMP2 hence new synthesis of TIMP2 may reflect compensation for increased MMP2 synthesis or activity in Dupuytren's disease or may fine-tune MMP activity.

Label-free quantification and pathway analysis identified TGFβ as a likely upstream regulator of a subset of proteins more abundant in Dupuytren's tissue. Several studies have demonstrated the presence of TGFβ in Dupuytren's disease with each isoform shown to be present by immunohistochemistry (Badalamente et al., 1996; Berndt et al., 1995; Bianchi et al., 2015; Ratajczak-Wielgomas et al., 2012) and each mRNA identified by RT-PCR or in-situ hybridization (Berndt et al., 1995; Krause et al., 2011; Ratajczak-Wielgomas et al., 2012; Zhang et al., 2008). Activation of the SMAD pathway indicates an active role for TGFβ in the disease process (Krause et al., 2011) hence it is highly feasible that TGFβ regulates expression of a subset of matricellular and cellular proteins in Dupuytren's disease.

Reactome pathways for Dupuytren's tissue after label-free quantification included those relating to extracellular matrix/collagen and the immune system. When normalization was carried out according to the total ion chromatogram, rather than wet weight of tissue, the top reactome pathways for Dupuytren's retained descriptors relating to the immune system, whereas those relating to extracellular matrix/collagen were associated with normal PF. The increased abundance of proteins related to an immune response seems consistent with a known inflammatory response in Dupuytren's disease (Mayerl et al., 2016) although a role for neutrophils has not been previously identified in Dupuytren's; indeed no neutrophil elastase positive cells were identified by immunohistochemistry in Dupuytren's nodules (Verjee et al., 2013). The altered association of extracellular matrix/collagens pathways with Dupuytren's tissue or normal PF depending on the normalization method indicates that the extracellular matrix/collagens may be more extractable from Dupuytren's tissue than normal PF, perhaps due to more recent synthesis and hence a reduced extent of protein crosslinking. Both tissues, particularly Dupuytren's cord contain fibrillar type I collagen and extracellular matrix but these terms are more associated with Dupuytren's tissue when normalizing to the wet weight of tissue. Active ECM protein synthesis and turnover in Dupuytren's disease is highlighted by the heavy isotope labelling results (Figs 4-5) and is consistent with the fibroproliferative disease process.

Proteins more abundant in normal PF included those involved in muscle filament sliding such as myosin light chain 2 (MYL2), myosin light chain 3 (MYL3) and myosin heavy chain 7 (MYH7). MYH7 neopeptides were also uniquely identified in normal PF (Table 5). Whilst the presence of these proteins may reflect a potential contamination from surrounding tissues, other studies have also identified transcripts more usually associated with muscle as being present in rat tendon (Mueller et al., 2016) and human Achilles (Peffers et al., 2015). Pathways relating to muscle formation were previously shown to be associated with proteins more abundant in the interfascicular matrix (endotendon) of equine SDFT than in

the collagenous fascicles (Thorpe et al., 2016). Thorpe et. al. obtained samples from the mid-metacarpal tendon region, far from any muscle, and utilised laser capture microdissection to prepare samples; hence contamination from surrounding tissues, or a long-range interdigitation of the myotendinous junction, seems unlikely. Ligament can contain a broader interfascicular matrix than tendon (Kharaz et al., 2018) hence muscle-related proteins in normal PF may arise from the interfascicular matrix and play a physiological role therein. The presence of proteins more usually associated with cartilage, such as cartilage intermediate layer protein 1 (CILP) and chondroadherin (CHAD) in normal PF, is consistent with previous findings of ourselves and others ligament, and may reflect the fibrocartilaginous nature of ligament regionally or throughout (Kharaz et al., 2016; Little et al., 2014). Several CILP neopeptides were identified in normal PF samples likely reflecting the abundance and turnover of CILP in ligament.

Myocilin was also more abundant in normal PF and myocilin neopeptides were uniquely identified in normal PF tissue (Table 5). Myocilin is found in the trabecular network of the eye and mutations are common in glaucoma (Wang et al., 2019). However myocilin has been previously identified in collagenous tissue, being enriched in male as compared to female anterior cruciate ligament (Little et al., 2014) and being identified within cells of the collagenous annulus fibrosus of the intervertebral disc (Gruber et al., 2006). Interestingly myocilin has been reported to modulate Wnt signalling (Kwon et al., 2009) whilst dysregulated Wnt signalling has been associated with Dupuytren's disease (Becker et al., 2016). Insufficient myocilin in Dupuytren's tissue may therefore promote pro-fibrotic Wnt signalling. TIMP3 has been shown to interact with myocilin to regulate MMP2 activity (Joe et al., 2017) and a dearth of myocilin in Dupuytren's tissue may result in a corresponding increase in MMP2 activity.

None of the neopeptides had incorporated heavy label, so were likely to have originated from the tissue itself. Several tenascin X (TNXB) neopeptides were identified in normal PF media and tissue, although tenascin X itself was not more abundant in normal PF according to the label-free analysis. Tenascin-X is a trimeric protein that plays a structural role in tissues interacting with fibrillar and FACIT collagens, as well as potentially regulating TGFβ bioavailability (Valcourt et al., 2015). Label-free analysis identified tenascin-C (TNC) as more abundant in Dupuytren's tissue and media. Tenascin-C is a hexameric matricellular protein that binds fibronectin, unlike tenascin-X and is expressed in embryonic tissues, tendon and numerous disease processes including lung and kidney fibrosis (Midwood et al., 2016). Tenascin-C often displays reciprocal expression to tenascin-X (Valcourt et al., 2015). The TNXB neopeptides in normal PF could represent a particular fragmentation process occurring during explant culture in ligament alone, or reflect the normal physiology of healthy ligament.

There was a striking enrichment of neopeptides from periostin (POST) in Dupuytren's media and tissue. Periostin can influence collagen fibrillogenesis, has been previously identified in periosteum, ligament, tendon and skin and is an emerging biomarker for pathological conditions (Kii, 2019). A previous study found that periostin transcripts were more abundant in Dupuytren's cord than normal PF by microarray analysis, qRT-PCR and in-situ hybridization whilst periostin protein was more abundant by Western blotting and immunohistochemistry (Vi et al., 2009). A separate study showed stronger periostin staining by immunohistochemistry in Dupuytren's tissue than in palmar fascia from carpal tunnel patients, with localized staining adjacent to α-SMA positive myofibroblasts and stronger staining in earlier compared to more advanced disease stages (Ratajczak-Wielgomas et al., 2012). In the present study, utilizing a mixture of stage 2 and stage 4 (Tubiana) Dupuytren's samples, we did not identify periostin as being more abundant in Dupuytren's tissue by label-free proteomics and a prior proteomics study comparing residual disease stage Dupuytren's tissue to adjacent unaffected palmar fascia similarly did not detect differential abundance of periostin (Kraljevic Pavelic et al., 2009). The neopeptides identified in the present study could have arisen from fragmentation over the course of the explant culture carried out for metabolic labelling, or from prior fragmentation within the tissue during disease progression.

There were numerous collagen (I) neopeptides present in normal PF and Dupuytren's tissue. None of the neopeptides corresponded to the MMP cleavage site in collagen (I), indicating that the peptides likely arose from later gelatinase activity. Only one alpha-1(I) chain neopeptide was present in at least three Dupuytren's cord and nodule samples, whilst for normal PF there was only one alpha-1(I) chain and two alpha-2(I) chain neopeptides that were present in at least three samples. New type I collagen synthesis in Dupuytren's tissue and media was confirmed by radio- and heavy-isotope labelling approaches, whilst the label-free analysis indicated that the alpha-2(I) chain (COL1A2), but not the alpha-1(I) chain (COL1A1) was more abundant in Dupuytren's tissue and media. This could reflect differences in extractability of previously synthesised heterotrimeric and homotrimeric collagen (I) molecules due to altered crosslinking (Pfeiffer et al., 2005). In this study, we used an extraction method for the insoluble pellet previously shown to increase the identification of collagenous proteins (Ashraf Kharaz et al., 2017) However, it may be that pepsinisation of the insoluble pellet (Peffers et al., 2014) to break mature crosslinks between telopeptides would have released more homotrimeric collagen (I), and hence alpha-1(I) chain (COL1A1) peptides from Dupuytren's tissue.

In conclusion, we have shown that Dupuytren's tissue actively synthesizes both homotrimeric and heterotrimeric type I collagen as well as MMP3 and TIMP2, supporting our hypothesis of a continual abnormal production of ECM proteins in Dupuytren's. Label-free proteomics implicated the TGFβTGFβ pathway in the profile of matrisomal proteins in Dupuytren's tissue whilst a lack of myocilin could contribute to aberrant Wnt signalling in Dupuytren's disease. The continual synthesis of collagen-1, MMPs and TIMPs together with TGFβ and Wnt pathway activation could therefore contribute to disease recurrence by promoting persistent collagen deposition and tissue remodeling.

Author contributions

Conceptualization: EGC-L. Funding acquisition: EGC-L. Resources: GCh, DB, RP, EVC, PDC. Methodology: KAW, GCo, KJL, EGC-L. Investigation: KAW, GCo, KJL, EB, DS, AC, JAG. Data curation: KAW, GCo, KJL, EB, DS, EGC-L. Project administration: RP, EVC, PDC, EGC-L. Supervision: EVC, PDC, EGC-L. Formal Analysis: KAW, GCo, KJL, EB, EGC-L. Visualization: KAW, GCo, KJL, EB, EGC-L. Writing – original draft: EGC-L. Writing – review & editing: KAW, GCo, KJL, EB, DS, JAG, GCh, DB, RP, EVC, PDC, EGC-L.

Acknowledgements

The assistance of the surgical teams and research nurses at the Royal Liverpool and Broadgreen University Hospitals NHS Trust and the Warrington and Halton Hospitals NHS Foundation Trust, as well as the contribution of the patients donating samples for the study is gratefully acknowledged. The authors would like to thank the staff at the Philip Leverhulme Equine Hospital and the Small Animal Teaching Hospital, as well as the owners that donated tissue for use in research. The authors are also grateful for the assistance of Professor Rob Beynon for advice on study design and data analysis and Professor Mandy Peffers in providing advice, a protocol and template for the neopeptide analysis. The invaluable assistance of Mr Adrian Chojnowski at the Norfolk and Norwich University Hospitals NHS Foundation Trust, and Dr Graham Riley and Professor Ian Clark at the University of East Anglia in providing human surgical samples (REC 10/H0310/03) early in the study is gratefully acknowledged.

This study was funded by the UK Medical Research Council (MRC) (MR/J002909) and the Dowager Countess Eleanor Peel Trust (DCEPT) (#148). KJL was supported by the Marjorie Forrest Bequest and by the Institute of Ageing and Chronic Disease at the University of Liverpool and now by MRC (MR/R00319X/1).

ELB is supported by Versus Arthritis (21809). JAG was supported by The Medical Research Council Versus Arthritis Centre for Integrated Research into Musculoskeletal Ageing (CIMA).

References

Akiel, M., C. Guo, X. Li, D. Rajasekaran, R.G. Mendoza, C.L. Robertson, N. Jariwala, F. Yuan, M.A. Subler, J. Windle, D.K. Garcia, Z. Lai, H.H. Chen, Y. Chen, S. Giashuddin, P.B. Fisher, X.Y. Wang, and D. Sarkar. 2017. IGFBP7 Deletion Promotes Hepatocellular Carcinoma. *Cancer Res*. 77:4014-4025.

Ali, O.J., E.J. Comerford, P.D. Clegg, and E.G. Canty-Laird. 2018. Variations during ageing in the three-dimensional anatomical arrangement of fascicles within the equine superficial digital flexor tendon. *Eur Cell Mater*. 35:87-102.

Angi, M., H. Kalirai, S. Prendergast, D. Simpson, D.E. Hammond, M.C. Madigan, R.J. Beynon, and S.E. Coupland. 2016. In-depth proteomic profiling of the uveal melanoma secretome. *Oncotarget*. 7:49623-49635.

Ashraf Kharaz, Y., D. Zamboulis, K. Sanders, E. Comerford, P. Clegg, and M. Peffers. 2017. Comparison between chaotropic and detergent-based sample preparation workflow in tendon for mass spectrometry analysis. *Proteomics*. 17.

Augoff, K., K. Ratajczak, J. Gosk, R. Tabola, and R. Rutowski. 2006. Gelatinase A activity in Dupuytren's disease. *J Hand Surg Am*. 31:1635-1639.

Badalamente, M.A., S.P. Sampson, L.C. Hurst, A. Dowd, and K. Miyasaka. 1996. The role of transforming growth factor beta in Dupuytren's disease. *J Hand Surg Am*. 21:210-215.

Becker, K., S. Siegert, M.R. Toliat, J. Du, R. Casper, G.H. Dolmans, P.M. Werker, S. Tinschert, A. Franke, C. Gieger, K. Strauch, M. Nothnagel, P. Nurnberg, H.C. Hennies, and G. German Dupuytren Study. 2016. Meta-Analysis of Genome-Wide Association Studies and Network Analysis-Based Integration with Gene Expression Data Identify New Suggestive Loci and Unravel a Wnt-Centric Network Associated with Dupuytren's Disease. *PLoS One*. 11:e0158101.

Berndt, A., H. Kosmehl, U. Mandel, U. Gabler, X. Luo, D. Celeda, L. Zardi, and D. Katenkamp. 1995. TGF beta and bFGF synthesis and localization in Dupuytren's disease (nodular palmar fibromatosis) relative to cellular activity, myofibroblast phenotype and oncofetal variants of fibronectin. *Histochem J*. 27:1014-1020.

Bianchi, E., S. Taurone, L. Bardella, A. Signore, E. Pompili, V. Sessa, C. Chiappetta, L. Fumagalli, C. Di Gioia, F.S. Pastore, S. Scarpa, and M. Artico. 2015. Involvement of pro-inflammatory cytokines and growth factors in the pathogenesis of Dupuytren's contracture: a novel target for a possible future therapeutic strategy? *Clin Sci (Lond)*. 129:711-720.

Brickley-Parsons, D., M.J. Glimcher, R.J. Smith, R. Albin, and J.P. Adams. 1981. Biochemical changes in the collagen of the palmar fascia in patients with Dupuytren's disease. *J Bone Joint Surg Am*. 63:787-797.

Clements, D.N., S.D. Carter, J.F. Innes, W.E. Ollier, and P.J. Day. 2008. Gene expression profiling of normal and ruptured canine anterior cruciate ligaments. *Osteoarthritis Cartilage*. 16:195-203.

Craxford, S., and P.G. Russell. 2016. Dupuytren's disease. *Surgery (Oxford)*. 34:139-143.

Dibenedetti, D.B., D. Nguyen, L. Zografos, R. Ziemiecki, and X. Zhou. 2011. Prevalence, incidence, and treatments of Dupuytren's disease in the United States: results from a population-based study. *Hand*. 6:149-158.

Dienes, Z. 2014. Using Bayes to get the most out of non-significant results. *Frontiers in Psychology*. 5.

Ehrlich, H.P., H. Brown, and B.S. White. 1982. Evidence for type V and I trimer collagens in Dupuytren's Contracture palmar fascia. *Biochem Med*. 28:273-284.

Evdokimova, V., C.E. Tognon, T. Benatar, W. Yang, K. Krutikov, M. Pollak, P.H. Sorensen, and A. Seth. 2012. IGFBP7 binds to the IGF-1 receptor and blocks its activation by insulin-like growth factors. *Sci Signal*. 5:ra92.

Forrester, H.B., P. Temple-Smith, S. Ham, D. de Kretser, G. Southwick, and C.N. Sprung. 2013. Genome-wide analysis using exon arrays demonstrates an important role for expression of extra-cellular matrix, fibrotic control and tissue remodelling genes in Dupuytren's disease. *PLoS One*. 8:e59056.

797 Fukui, N., Y. Katsuragawa, A. Kawakami, H. Sakai, H. Oda, and K. Nakamura. 2001. Metabolic activity in
798 disrupted human anterior cruciate ligament. Evaluation of procollagen mRNA expression in 29
799 patients. *Joint Bone Spine*. 68:318-326.
800 Grazina, R., S. Teixeira, R. Ramos, H. Sousa, A. Ferreira, and R. Lemos. 2019. Dupuytren's disease: where do
801 we stand? *EFORT Open Rev*. 4:63-69.
802 Gruber, H.E., J.A. Ingram, and E.N. Hanley, Jr. 2006. Cellular immunohistochemical localization of the
803 matricellular protein myocilin in the intervertebral disc. *Biotech Histochem*. 81:119-124.
804 Hammond, D.E., J.D. Kumar, L. Raymond, D.M. Simpson, R.J. Beynon, G.J. Dockray, and A. Varro. 2018.
805 Stable Isotope Dynamic Labeling of Secretomes (SIDLS) Identifies Authentic Secretory Proteins
806 Released by Cancer and Stromal Cells. *Molecular & cellular proteomics : MCP*. 17:1837-1849.
807 Hindocha, S., D.A. McGrouther, and A. Bayat. 2009. Epidemiological evaluation of Dupuytren's disease
808 incidence and prevalence rates in relation to etiology. *Hand*. 4:256-269.
809 Hindocha, S., J.K. Stanley, J.S. Watson, and A. Bayat. 2008. Revised Tubiana's staging system for assessment
810 of disease severity in Dupuytren's disease-preliminary clinical findings. *Hand*. 3:80-86.
811 Joe, M.K., R.L. Lieberman, N. Nakaya, and S.I. Tomarev. 2017. Myocilin Regulates Metalloprotease 2 Activity
812 Through Interaction With TIMP3. *Invest Ophthalmol Vis Sci*. 58:5308-5318.
813 Johnston, P., A.J. Chojnowski, R.K. Davidson, G.P. Riley, S.T. Donell, and I.M. Clark. 2007. A Complete
814 Expression Profile of Matrix-Degrading Metalloproteinases in Dupuytren's Disease. *The Journal of*
815 *Hand Surgery*. 32:343-351.
816 Johnston, P., D. Larson, I.M. Clark, and A.J. Chojnowski. 2008. Metalloproteinase gene expression correlates
817 with clinical outcome in Dupuytren's disease. *J Hand Surg Am*. 33:1160-1167.
818 Jung, J., G.W. Kim, B. Lee, J.W.J. Joo, and W. Jang. 2019. Integrative genomic and transcriptomic analysis of
819 genetic markers in Dupuytren's disease. *BMC Med Genomics*. 12:98.
820 Kharaz, Y.A., E.G. Canty-Laird, S.R. Tew, and E.J. Comerford. 2018. Variations in internal structure,
821 composition and protein distribution between intra- and extra-articular knee ligaments and
822 tendons. *J Anat*. 232:943-955.
823 Kharaz, Y.A., S.R. Tew, M. Peffers, E.G. Canty-Laird, and E. Comerford. 2016. Proteomic differences between
824 native and tissue-engineered tendon and ligament. *Proteomics*. 16:1547-1556.
825 Kii, I. 2019. Practical Application of Periostin as a Biomarker for Pathological Conditions. *Adv Exp Med Biol*.
826 1132:195-204.
827 Kilian, O., U. Pfeil, S. Wenisch, C. Heiss, R. Kraus, and R. Schnettler. 2007. Enhanced alpha 1(I) mRNA
828 expression in frozen shoulder and dupuytren tissue. *Eur J Med Res*. 12:585-590.
829 Kraljevic Pavelic, S., M. Sedic, K. Hock, S. Vucinic, D. Jurisic, P. Gehrig, M. Scott, R. Schlapbach, T. Cacev, S.
830 Kapitanovic, and K. Pavelic. 2009. An integrated proteomics approach for studying the molecular
831 pathogenesis of Dupuytren's disease. *The Journal of pathology*. 217:524-533.
832 Krause, C., P. Kloen, and P. Ten Dijke. 2011. Elevated transforming growth factor beta and mitogen-
833 activated protein kinase pathways mediate fibrotic traits of Dupuytren's disease fibroblasts.
834 *Fibrogenesis Tissue Repair*. 4:14.
835 Krefter, C., M. Marks, S. Hensler, D.B. Herren, and M. Calcagni. 2017. Complications after treating
836 Dupuytren's disease. A systematic literature review. *Hand Surg Rehabil*. 36:322-329.
837 Kwon, H.S., H.S. Lee, Y. Ji, J.S. Rubin, and S.I. Tomarev. 2009. Myocilin is a modulator of Wnt signaling. *Mol*
838 *Cell Biol*. 29:2139-2154.
839 Lam, W.L., J.M. Rawlins, R.O. Karoo, I. Naylor, and D.T. Sharpe. 2010. Re-visiting Luck's classification: a
840 histological analysis of Dupuytren's disease. *J Hand Surg Eur Vol*. 35:312-317.
841 Layton, T., and J. Nanchahal. 2019. Recent advances in the understanding of Dupuytren's disease.
842 *F1000Res*. 8.
843 Lee, K.J., P.D. Clegg, E.J. Comerford, and E.G. Canty-Laird. 2018. A comparison of the stem cell
844 characteristics of murine tenocytes and tendon-derived stem cells. *BMC Musculoskelet Disord*.
845 19:116.
846 Lee, K.J., E.J. Comerford, D.M. Simpson, P.D. Clegg, and E.G. Canty-Laird. 2019. Identification and
847 Characterization of Canine Ligament Progenitor Cells and Their Extracellular Matrix Niche. *J*
848 *Proteome Res*. 18:1328-1339.

Little, D., J.W. Thompson, L.G. Dubois, D.S. Ruch, M.A. Moseley, and F. Guilak. 2014. Proteomic differences between male and female anterior cruciate ligament and patellar tendon. *PLoS One*. 9:e96526.

Luck, J.V. 1959. Dupuytren's contracture; a new concept of the pathogenesis correlated with surgical management. *J Bone Joint Surg Am*. 41-A:635-664.

Makareeva, E., S. Han, J.C. Vera, D.L. Sackett, K. Holmbeck, C.L. Phillips, R. Visse, H. Nagase, and S. Leikin. 2010. Carcinomas Contain a Matrix Metalloproteinase–Resistant Isoform of Type I Collagen Exerting Selective Support to Invasion. *Cancer Res*. 70:4366-4374.

Mayerl, C., B. Del Frari, W. Parson, G. Boeck, H. Piza-Katzer, G. Wick, and D. Wolfram. 2016. Characterisation of the inflammatory response in Dupuytren's disease. *J Plast Surg Hand Surg*. 50:171-179.

Midwood, K.S., M. Chiquet, R.P. Tucker, and G. Orend. 2016. Tenascin-C at a glance. *J Cell Sci*. 129:4321-4327.

Mueller, A.J., S.R. Tew, O. Vasieva, P.D. Clegg, and E.G. Canty-Laird. 2016. A systems biology approach to defining regulatory mechanisms for cartilage and tendon cell phenotypes. *Scientific reports*. 6:33956.

Ng, M., D. Thakkar, L. Southam, P. Werker, R. Ophoff, K. Becker, M. Nothnagel, A. Franke, P. Nurnberg, A.I. Espirito-Santo, D. Izadi, H.C. Hennies, J. Nanchahal, E. Zeggini, and D. Furniss. 2017. A Genome-wide Association Study of Dupuytren Disease Reveals 17 Additional Variants Implicated in Fibrosis. *Am J Hum Genet*. 101:417-427.

Peffers, M.J., Y. Fang, K. Cheung, T.K. Wei, P.D. Clegg, and H.L. Birch. 2015. Transcriptome analysis of ageing in uninjured human Achilles tendon. *Arthritis Res Ther*. 17:33.

Peffers, M.J., C.T. Thorpe, J.A. Collins, R. Eong, T.K. Wei, H.R. Screen, and P.D. Clegg. 2014. Proteomic analysis reveals age-related changes in tendon matrix composition, with age- and injury-specific matrix fragmentation. *Journal of Biological Chemistry*. 289:25867-25878.

Pfeiffer, B.J., C.L. Franklin, F.H. Hsieh, R.A. Bank, and C.L. Phillips. 2005. Alpha 2(I) collagen deficient oim mice have altered biomechanical integrity, collagen content, and collagen crosslinking of their thoracic aorta. *Matrix Biol*. 24:451-458.

Ratajczak-Wielgomas, K., J. Gosk, J. Rabczynski, K. Augoff, M. Podhorska-Okolow, A. Gamian, and R. Rutowski. 2012. Expression of MMP-2, TIMP-2, TGF-beta1, and decorin in Dupuytren's contracture. *Connect Tissue Res*. 53:469-477.

Riester, S.M., D. Arsoy, E.T. Camilleri, A. Dudakovic, C.R. Paradise, J.M. Evans, J. Torres-Mora, M. Rizzo, P. Kloen, M.K. Julio, A.J. van Wijnen, and S. Kakar. 2015. RNA sequencing reveals a depletion of collagen targeting microRNAs in Dupuytren's disease. *BMC Med Genomics*. 8:59.

Robbins, J.R., and K.G. Vogel. 1994. Regional expression of mRNA for proteoglycans and collagen in tendon. *Eur J Cell Biol*. 64:264-270.

Shih, B., S. Watson, and A. Bayat. 2012. Whole genome and global expression profiling of Dupuytren's disease: systematic review of current findings and future perspectives. *Ann Rheum Dis*. 71:1440-1447.

Soreide, E., M.H. Murad, J.M. Denbeigh, E.A. Lewallen, A. Dudakovic, L. Nordsletten, A.J. van Wijnen, and S. Kakar. 2018. Treatment of Dupuytren's contracture: a systematic review. *Bone Joint J*. 100-B:1138-1145.

Sykes, B., B. Puddle, M. Francis, and R. Smith. 1976. The estimation of two collagens from human dermis by interrupted gel electrophoresis. *Biochem Biophys Res Commun*. 72:1472-1480.

Szklarczyk, D., A.L. Gable, D. Lyon, A. Junge, S. Wyder, J. Huerta-Cepas, M. Simonovic, N.T. Doncheva, J.H. Morris, P. Bork, L.J. Jensen, and C.V. Mering. 2019. STRING v11: protein-protein association networks with increased coverage, supporting functional discovery in genome-wide experimental datasets. *Nucleic Acids Res*. 47:D607-D613.

Tan, K., A.H.J. Withers, S.T. Tan, and T. Itinteang. 2018. The Role of Stem Cells in Dupuytren's Disease: A Review. *Plast Reconstr Surg Glob Open*. 6:e1777.

Ten Dam, E.J., M.M. van Beuge, R.A. Bank, and P.M. Werker. 2016. Further evidence of the involvement of the Wnt signaling pathway in Dupuytren's disease. *J Cell Commun Signal*. 10:33-40.

Thorpe, C.T., M.J. Peffers, D. Simpson, E. Halliwell, H.R. Screen, and P.D. Clegg. 2016. Anatomical heterogeneity of tendon: Fascicular and interfascicular tendon compartments have distinct proteomic composition. *Scientific reports*. 6:20455.

Tomasek, J.J., and C.J. Haaksma. 1991. Fibronectin filaments and actin microfilaments are organized into a fibronexus in Dupuytren's diseased tissue. *Anat Rec*. 230:175-182.

Turlo, A.J., A.J. Mueller-Breckenridge, D.E. Zamboulis, S.R. Tew, E.G. Canty-Laird, and P.D. Clegg. 2019. Insulin-like growth factor binding protein (IGFBP6) is a cross-species tendon marker. *Eur Cell Mater*. 38:123-136.

Ulrich, D., K. Hrynyschyn, and N. Pallua. 2003. Matrix metalloproteinases and tissue inhibitors of metalloproteinases in sera and tissue of patients with Dupuytren's disease. *Plast Reconstr Surg*. 112:1279-1286.

Valcourt, U., L.B. Alcaraz, J.Y. Exposito, C. Lethias, and L. Bartholin. 2015. Tenascin-X: beyond the architectural function. *Cell Adh Migr*. 9:154-165.

van Beuge, M.M., E.J. Ten Dam, P.M. Werker, and R.A. Bank. 2016. Matrix and cell phenotype differences in Dupuytren's disease. *Fibrogenesis Tissue Repair*. 9:9.

Verjee, L.S., K. Midwood, D. Davidson, D. Essex, A. Sandison, and J. Nanchahal. 2009. Myofibroblast distribution in Dupuytren's cords: correlation with digital contracture. *J Hand Surg Am*. 34:1785-1794.

Verjee, L.S., J.S. Verhoekx, J.K. Chan, T. Krausgruber, V. Nicolaidou, D. Izadi, D. Davidson, M. Feldmann, K.S. Midwood, and J. Nanchahal. 2013. Unraveling the signaling pathways promoting fibrosis in Dupuytren's disease reveals TNF as a therapeutic target. *Proc Natl Acad Sci U S A*. 110:E928-937.

Vi, L., L. Feng, R.D. Zhu, Y. Wu, L. Satish, B.S. Gan, and D.B. O'Gorman. 2009. Periostin differentially induces proliferation, contraction and apoptosis of primary Dupuytren's disease and adjacent palmar fascia cells. *Exp Cell Res*. 315:3574-3586.

Wang, H., M. Li, Z. Zhang, H. Xue, X. Chen, and Y. Ji. 2019. Physiological function of myocilin and its role in the pathogenesis of glaucoma in the trabecular meshwork (Review). *International journal of molecular medicine*. 43:671-681.

Wilkinson, J.M., R.K. Davidson, T.E. Swingler, E.R. Jones, A.N. Corps, P. Johnston, G.P. Riley, A.J. Chojnowski, and I.M. Clark. 2012. MMP-14 and MMP-2 are key metalloproteases in Dupuytren's disease fibroblast-mediated contraction. *Biochimica et Biophysica Acta (BBA) - Molecular Basis of Disease*. 1822:897-905.

Wilson, R., A.F. Diseberg, L. Gordon, S. Zivkovic, L. Tatarczuch, E.J. Mackie, J.J. Gorman, and J.F. Bateman. 2010. Comprehensive profiling of cartilage extracellular matrix formation and maturation using sequential extraction and label-free quantitative proteomics. *Molecular & cellular proteomics : MCP*. 9:1296-1313.

Worrell, M. 2012. Dupuytren's disease. *Orthopedics*. 35:52-60.

Wynn, T.A. 2008. Cellular and molecular mechanisms of fibrosis. *The Journal of pathology*. 214:199-210.

Ye, C., W. Hou, M. Chen, J. Lu, E. Chen, L. Tang, K. Hang, Q. Ding, Y. Li, W. Zhang, and R. He. 2020. IGFBP7 acts as a negative regulator of RANKL-induced osteoclastogenesis and oestrogen deficiency-induced bone loss. *Cell Prolif*. 53:e12752.

Zeisberg, M., and R. Kalluri. 2013. Cellular mechanisms of tissue fibrosis. 1. Common and organ-specific mechanisms associated with tissue fibrosis. *Am J Physiol Cell Physiol*. 304:C216-225.

Zhang, A.Y., K.D. Fong, H. Pham, R.P. Nacamuli, M.T. Longaker, and J. Chang. 2008. Gene expression analysis of Dupuytren's disease: the role of TGF-beta2. *J Hand Surg Eur Vol*. 33:783-790.

Zhang, W., E. Chen, M. Chen, C. Ye, Y. Qi, Q. Ding, H. Li, D. Xue, X. Gao, and Z. Pan. 2018. IGFBP7 regulates the osteogenic differentiation of bone marrow-derived mesenchymal stem cells via Wnt/beta-catenin signaling pathway. *FASEB J*. 32:2280-2291.

Supplementary Results

Variability in metabolic labelling between Dupuytren's tissue explants

Samples derived from 4 of 31 patients were insufficiently labelled for densitometric quantification. Some patients donated samples from more than one digit. In others, cord and nodule were distinct and hence processed separately.

For 2 patients gifting samples relating to different digits the sample from only the thumb (and not the ring/little or little finger) was labelled. For one patient neither the samples donated from the little or ring finger were labelled. No labelled samples from multiple digits from the same patient were obtained.

For 2 of 5 patients, with samples for which both cord and nodule were processed, only the nodule was sufficiently labelled for quantification. For samples for which both cord and nodule were processed, the mean value for the ratio was used for analyses.

Supplementary Figures

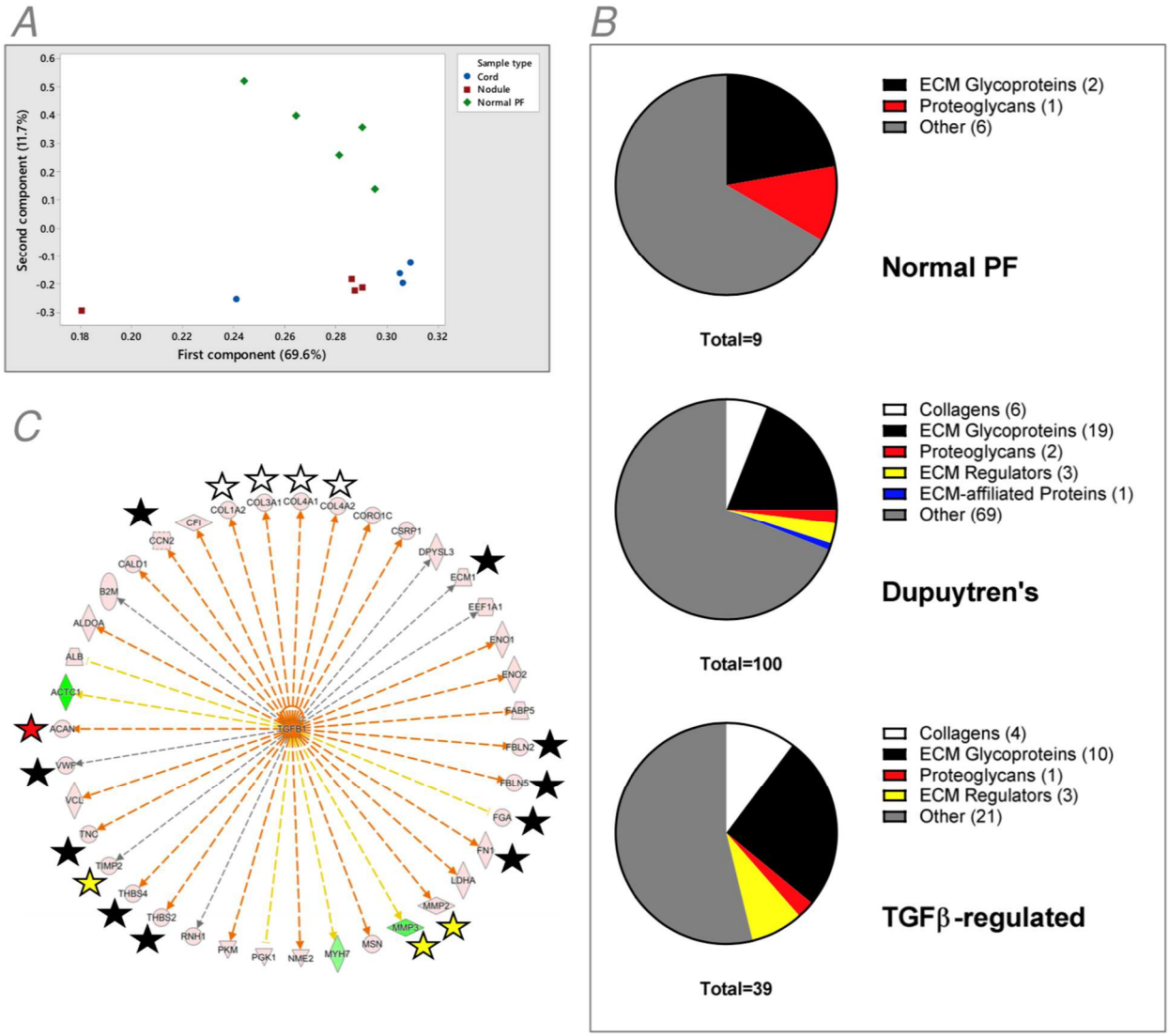

Supplementary Figure S1. Label-free proteomics analysis of normal palmar fascia (PF) and Dupuytren's explant media. A: Principal component analysis score plot grouped by tissue type. B: Enriched proteins in normal PF media, Dupuytren's media and those in Dupuytren's media predicted to be regulated by TGFβ, subdivided based on matrisomal classification. C: Ingenuity Pathway Analysis diagram highlighting matrisomal proteins within those predicted to be regulated by TGFβ. Red; increased abundance, green; decreased abundance, orange; predicted to lead to activation, blue; predicted to lead to inhibition, yellow; findings inconsistent with state of downstream molecule, grey; effect not predicted. Matrisomal proteins are indicated with a star (collagens; white, Extracellular Matrix [ECM] Glycoproteins; black, ECM-affiliated Proteins; blue, Proteoglycans; red, ECM Regulators; yellow, Secreted Factors; green).

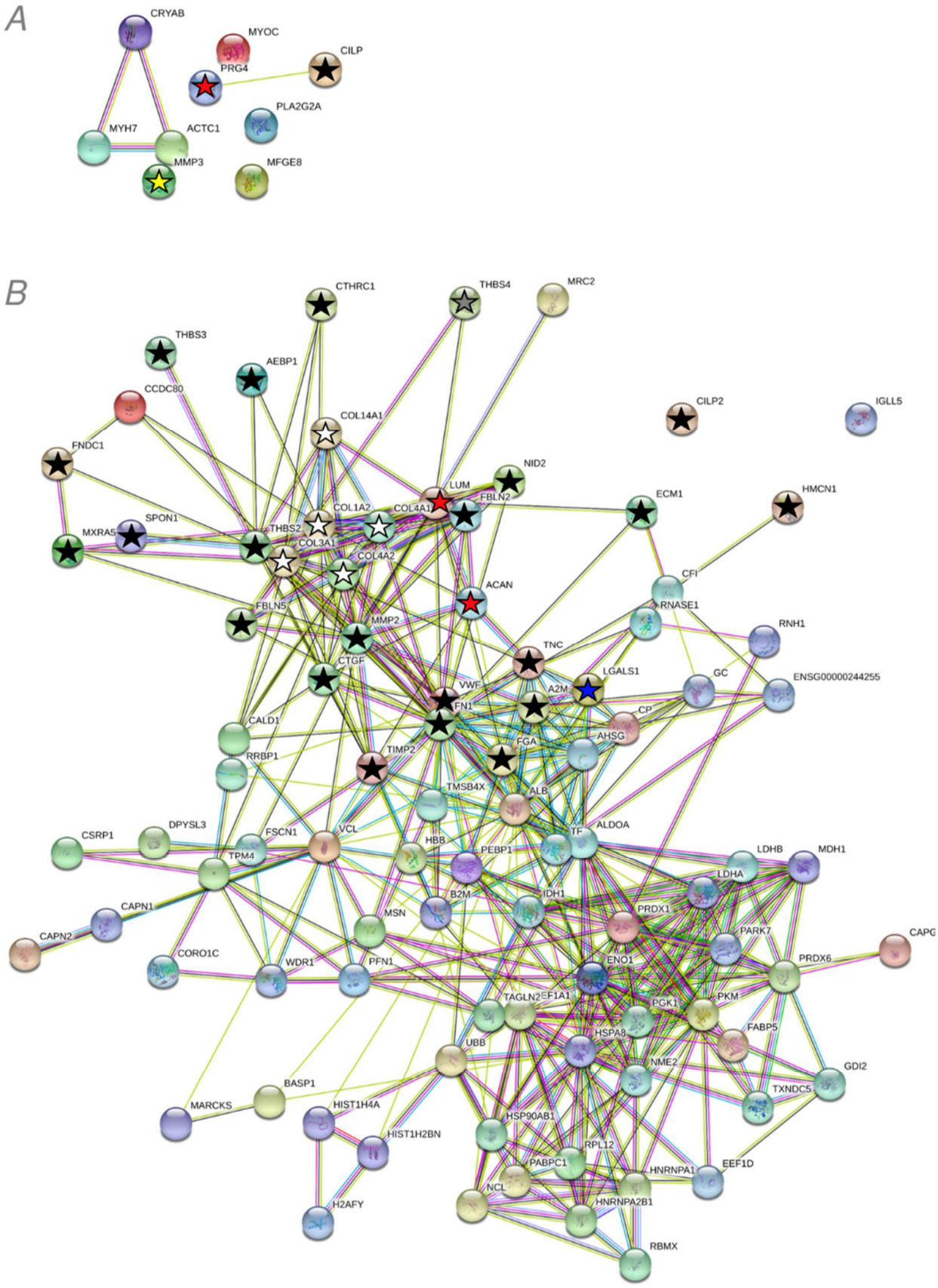

Supplementary Figure S2. STRING interaction networks for normal palmar fascia (PF) and Dupuytren's explant media. A: Interaction network for proteins enriched in normal PF explant media. B: Interaction network for proteins enriched in Dupuytren's explant media.

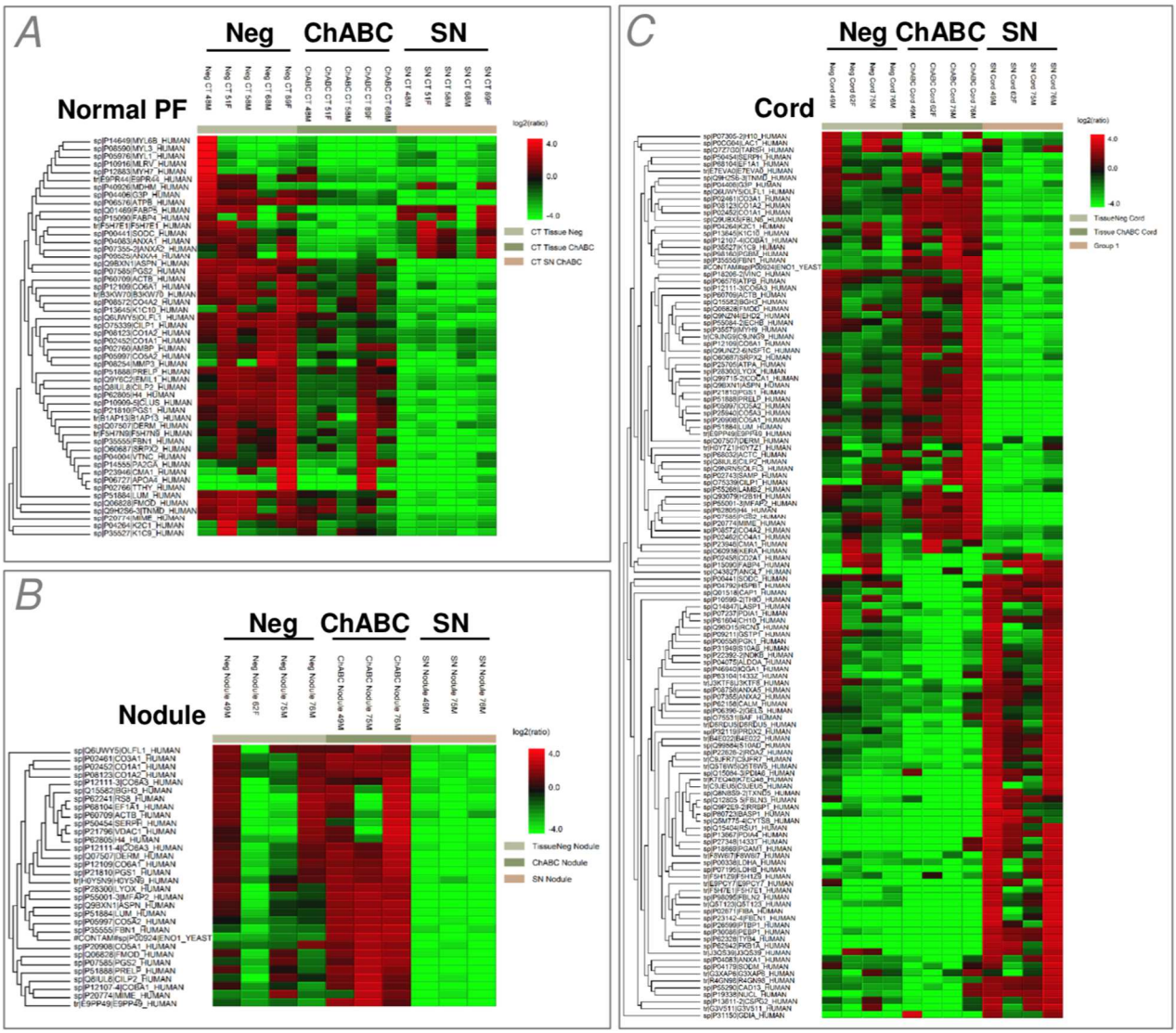

Supplementary Figure S3. Evidence for loss of proteins into the supernatant with chondroitinase ABC treatment. Heatmap of relative protein abundance in untreated (Neg) and chondroitinase ABC-treated (ChABC) samples as compared to the ChABC supernatant (SN) each normalised to equivalent tissue weight. A: Normal palmar fascia (PF). B: Dupuytren's nodule. C: Dupuytren's cord. The number of nodule samples was 3 rather than 4, as one ChABC -treated sample was misplaced.

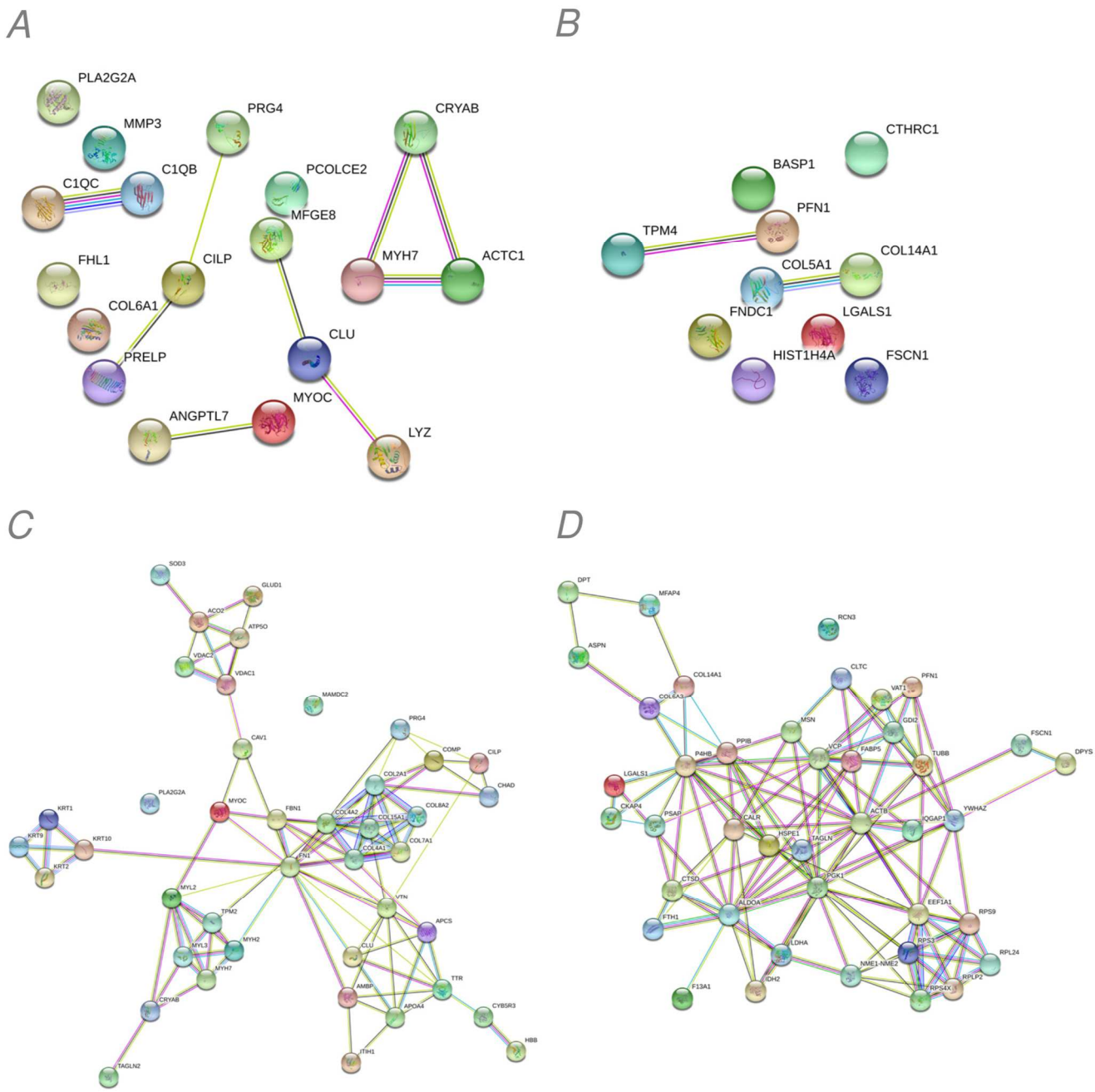

Supplementary Figure S4. STRING interaction networks for normal palmar fascia (PF) and Dupuytren's explant media for proteins normalised using total ion chromatogram. A: Interaction network for proteins enriched in normal PF explant media. B: Interaction network for proteins enriched in Dupuytren's explant media. C: Interaction network for proteins enriched in normal PF explant tissue. D: Interaction network for proteins enriched in Dupuytren's explant tissue.